

Molecular Switches Incorporating the Adducts Among Viologen unints and both Copper Bis (ethylacetoacetate) and Copper Bis(ethyl 4-chloroacetoacetate)

Ahmed A. Alibrahimi ¹, Wathiq Sattar Abdul-Hassan¹

¹Department of chemistry, College of science, University of Thi-Qar, 64001 Nassiria, Iraq Email ID: ahmedoudah501@gmail.com, https://orcid.org/0000-0002-3271-9015

Email ID: Wathiq-a.chem@sci.utq.edu.iq, https://orcid.org/0000-0003-1297-3822

ABSTRACT

This work investigates the preparation and analysis of Cu (II) complexes CuE and CuECl, along with their axial adducts formed through coordination with 4,4'-bipyridine CuEbpy and CuEClbpy and mono-viologen ($C_1V^+.PF_6^-$) CuEC $_1V^+.PF_6^-$ and CuEClC $_1V^+.PF_6^-$. In addition, reduction reactions were performed on the bis-viologen-based adduct complexes (CuEV $_2^{2+}.2PF_6^-$) using activated zinc powder under an inert atmosphere, leading to the generation of redox-active molecular switches centered on the viologen units. All synthesized Cu(II) complexes were comprehensively characterized using a suite of analytical techniques, including FT-IR, mass spectrometry, thermal analysis (TGA), X-ray diffraction (XRD), energy-dispersive X-ray spectroscopy (EDX), UV-Visible spectroscopy in various solvents, and electrochemical measurements. These characterizations confirm the successful formation of the target complexes and provide insight into their structural, optical, and redox properties.

KEYWORDS: Viologen, Molecular switches, Copper bis(β-diketone), π -dimer, 4,4'-Bipyridine, Bisviologen, Adduct

How to Cite: Ahmed A. Alibrahimi, Wathiq Sattar Abdul-Hassan, (20yy) Molecular Switches Incorporating the Adducts Among Viologen unints and both Copper Bis (ethylacetoacetate) and Copper Bis(ethyl 4-chloroacetoacetate), Vascular and Endovascular Review, Vol.8, No.6s, 151-182.

INTRODUCTION

Viologens consist of bipyridine salts where one or both nitrogen atoms carry a quaternary charge. Formally, they are referred to as 1,1'-disubstituted or 4,4'-bpy salts. When both substituents are methyl groups (R = methyl), the resulting dication is commonly known as methyl viologen ^[1,2]. Viologens are compounds is easily reduced to the radical mono cation and produce violet color. They can change color reversibly many times through <u>reduction and oxidation</u>. The viologen is a widely used <u>herbicide</u>, as early in the 1930 ^[3]. The viologen derivatives exist Viologen (V) exhibits three distinct redox states: the dication (V^{2+}), the radical cation (V^{++}), and the fully reduced neutral form (V^{0-}), as illustrated in Scheme 1.:

$$R-N$$
 $N-R$
 $+e^{-}$
 $R-N$
 $N-R$
 N

Scheme 1: Three common viologen redox states [4].

Molecular switch is a molecule that is able to convert reversibly between at least two stable states or several stable states by applying an external stimulus like thermal, chemical, electrical

optical et cetera. What is interesting is that the passage of a molecule from one state to another must be accompanied by a property of the molecule that can be read or seen by spectroscopic techniques such as NMR, UV Visible also by voltammetry electrochemical techniques [5].

The main objective of this study was to synthesize and characterize adduct complexes CuEbpy, CuEC₁V⁺.PF₆⁻, and CuEClC₁V⁺.PF₆⁻ originating from the Cu(II) complexes of ethyl acetoacetate (CuE) and ethyl 4-chloroacetoacetate (CuECl) in combination with bpy. Additionally, the research aimed to monitor the formation of these adducts in the solid state, as well as the assembly of CuEV₂²⁺.2PF₆⁻, which involves both Cu(II) precursors and the bis-viologen derivative V₂²⁺.2PF₆⁻. The study further investigated the redox-induced π -dimerization behavior of the coordinated bis-viologen moieties within CuEV₂²⁺.2PF₆⁻.

EXPERIMENTAL

Materials and Methods

Chemicals materials and Instrumentation

Chemicals reagents and solvents were very purification and their sources from certified and discreet chemical companies. These chemicals materials were used in the practical study without the need for re-purification. They are described as

follows: Ethyl4-chloroacetoacetate, Ethyl acetoacetate, bpy, 1,3-Dibromo propane, Copper acetoacetate, Absolute methanol, Ethanol, Acetonitrile, Acetone, Hexane, Dichloromethane and Dimethylformamide were from Chem-Lab/Belgium. Dimethyl sulfoxide, Benzene and Ethyl acetate were from Romil/England.

FT-IR spectra were obtained in the 500–4000 cm⁻¹ range using a SHIMADZU/FT-IR Affinity spectrophotometer with KBr pellets. UV-Vis absorption spectra were measured on a T90+ UV-Vis spectrometer (PG Instruments Ltd.) with 1 cm quartz cuvettes. Thermogravimetric analyses of the metal complexes were performed using an SDT Q600 V20.9 Build 20. XRD patterns were recorded with a Panalytical diffractometer employing Cu Kα radiation in Iran. ¹H-NMR spectra were acquired on a 400 MHz BRUKER spectrometer using DMSO-d₆ as solvent. Mass spectra were collected with a 5973 Network Mass Selective Detector (Agilent Technologies, HP) operating with an EI source at 70 eV. Electrochemical measurements were carried out using a Potentiostat/Galvanostat EIS Analyzer. Melting points were determined with a Cole-Parmer MP-200D apparatus (UK design, PRC assembly).

PREPARATION OF METHODS

Synthesis of CuE and CuECl complexes

To synthesize the CuE complex, ethyl acetoacetate (3 mL, 23.536 mmol, 2 equivalents) was dissolved in 1 mL of ethanol and added drop wise to a solution of copper(II) acetate monohydrate (2.179 g, 11.768 mmol, 1 equivalent) dissolved in 10 mL of ethanol. The addition was carried out over a period of 20 minutes with constant stirring. The resulting mixture was stirred for an additional 2 hours at room temperature, then heated to 60 °C and maintained at this temperature for 2 hours under continuous stirring. A solid precipitate was formed during the reaction. For the synthesis of the CuECl complex, ethyl 4-chloroacetoacetate (2 mL, 14.800 mmol, 2 equivalents) was dissolved in 1 mL of ethanol and added gradually over 10 minutes to a solution of Cu (II) acetate monohydrate (1.344 g, 7.400 mmol, 1 equivalent) dis-solved in 10ml of a CH₃OH–H₂O mixture, then heated to 60 °C for 2 hours with continuous stirring to ensure complete reaction and complex formation. In both cases, After vacuum filtration, the precipitate was thoroughly washed with water and methanol, followed by drying under reduced pressure. The CuE complex was obtained as a green crystalline solid with a yield of 2.00 g (52%) and a melting point of 195–197 °C. The CuECl complex was obtained as a brown solid with a yield of 2.3302 g (81%) and a melting point of 170–172 °C. Both complexes exhibit excellent solubility in polar and moderately polar solvents, including water, methanol, ethanol, acetonitrile, acetone, dichloromethane, ethyl acetate, benzene, DMF, and DMSO, which facilitates further characterization and potential applications in solution-based systems ^[6].

Scheme 2: Syntheses of CuE and CuECl.

Synthesis of CuEbpy and CuEClbpy complexes as adduct

To prepare the CuEbpy complex, a solution of the previously synthesized CuE complex (0.400 g, 1.252 mmol, 1 equivalent) was dissolved in a minimal volume of DMF and added, under continuous stirring, to a solution of bpy (0.980 g, 6.26 mmol, 5 equivalents), also dis-solved in the least possible of DMF. Mixture was stirrer at Lab tem. for 48 h to ensure complete coordination and adduct formation. Similarly, for the synthesis of the CuEClbpy complex, a solution of CuECl (1.000 g, 2.567 mmol, 1 equivalent) was dissolved in the minimum amount of DMF and added with stirring to a solution of 4,4'-bipyridine (2.000 g, 12.84 mmol, 5 equivalents), previously dissolved in a minimal volume of DMF. The resulting mixture was also stirred at ambient temperature for 48 hours. In both syntheses, the resulting precipitates were collected by vacuum filtration, washed thoroughly with dichloromethane to remove unreacted organic residues, and dried under reduced pressure. The CuEbpy adduct was obtained as a greenish-yellow solid with a yield of 0.200 g (33%), and a melting point of 142–144 °C. The CuEClbpy adduct was isolated as a brown solid with a yield of 0.710 g (39%), and a melting point of 197–199 °C. Both adduct complexes exhibit good solubility in a wide range of solvents, including water, methanol, ethanol, acetonitrile, acetone, dichloromethane, ethyl acetate, benzene, DMF, and DMSO, which is advantageous for subsequent characterization and potential applications in solution-based coordination systems ^[7].

Scheme 3: Syntheses of CuEbpy and CuEClbpy.

Synthesis of CuEC₁V⁺·PF₆⁻ and CuEClC₁V⁺·PF₆⁻ complexes as adduct

The synthesis of the viologen-based adduct complexes $CuEC_1V^+\cdot PF_6^-$ and $CuEClC_1V^+\cdot PF_6^-$ was carried out by reacting the corresponding copper(II) β -ketoester complexes with 1-methyl-4,4'-bipyridinium hexafluorophosphate $(C_1V^+\cdot PF_6^-)$ in DMF under ambient conditions. For the synthesis of $CuEC_1V^+\cdot PF_6^-$, a solution of $C_1V^+\cdot PF_6^-$ (1.230 g, 3.89 mmol, 5 equivalents) was dissolved in 1 mL of DMF and added gradually, over the course of one minute with continuous stirring, to a solution of CuE (0.625 g, 1.95 mmol, 1 equivalent) previously dissolved in 3 mL of (DMF). The contents of the reaction were mixed by agitation inside a firmly closed volumetric flask at Lab tem. for 45 days. Reaction progress was monitored by (TLC) using a mobile phase of MeCN:H₂O: KNO₃ (10:1:1, v/v/v). Upon completion, The formed precipitate was isolated through filtration and subsequently dried under to yield the complex $CuEC_1V^+\cdot PF_6^-$ as a light green solid (yield: 0.180 g, 15%), with a melting point of 168 °C.

Similarly, for preparation of $CuEClC_1V^+\cdot PF_6^-$, from $C_1V^+\cdot PF_6^-$ (1.400 g , 2.77mmol, 5 equivalents) in 1ml of DMF was added gradually over one minute, under stirring, to of CuECl (0.860 g, 2.221 mmol, 1 equivalent) dissolved in 4 mL of DMF. The mixture was stirred in a sealed volumetric flask at room temperature for 45 days. The reaction was monitored by TLC using the same eluent system. The precipitate formed was filtered and and then subjected to vacuum drying to obtain of $CuEClC_1V^+\cdot PF_6^-$ as a soft brown solid (yield: 0.087 g, 7.5%), with a melting point of 175-177 °C. Both complexes exhibited low solubility in water, methanol, ethanol, acetonitrile, DMF, and DMSO, and were insoluble in acetone, dichloromethane (DCM), ethyl acetate (EtOAc), and benzene (C_6H_6) $^{[7]}$.

R= Ethyl acetoacetate or Cl: Ethyl4-chloroacetoacetate

$$C_1V^+$$
. $PF_6^ C_1V^+$. PF_6^- 8 %

Scheme 4: Synthesis of CuEC₁V⁺.PF₆⁻ and CuEC₁C₁V⁺.PF₆⁻ complex.

RESULTS AND DISCUSSION

Characterization of Cu²⁺-complexes

FT-IR spectroscopy of Cu²⁺ complexes

Fourier-transform infrared spectra were recorded for the complexes CuE and CuECl, along with their respective adducts: CuEbpy, CuEClbpy, CuEC $_1V^+$.PF $_6^-$ and CuEClC $_1V^+$.PF $_6^-$ are recorded and presented in figure 1 and data are listed table 1.

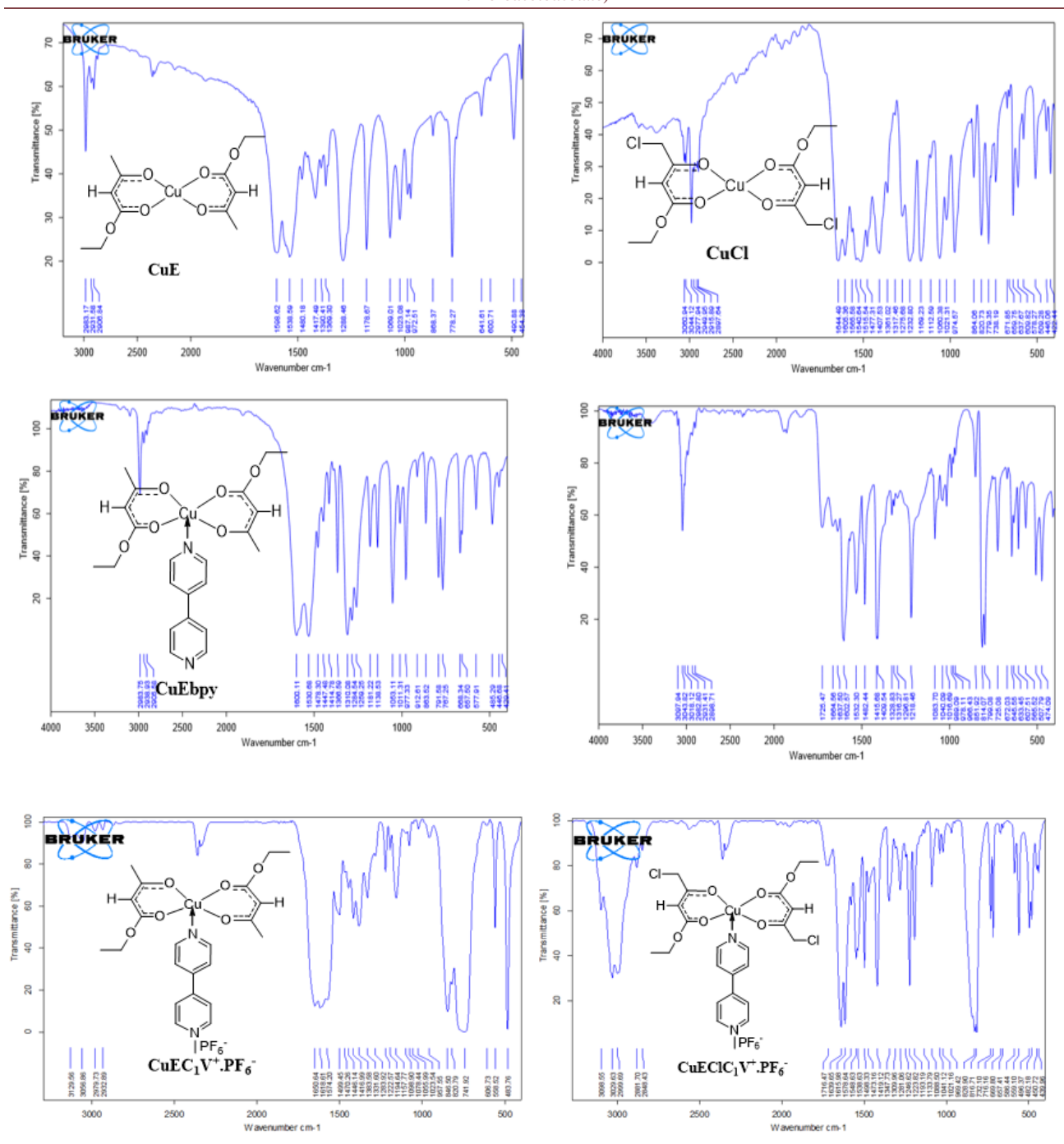


Table 1: Important FT-IR data of Cu²⁺ complexes.

Compound	arom atic and olefini c C-H stretc hing	aliph atic C-H stret chig	coupled with C=C C=O	aro mat ic and olef inic C- H ben din g	alipha tic C-H bendi ng	C-N	C-O	PF6 Str etc hin g	Stretchi ng C-C	Be ndi ng C-Cl	Cu - O	Cu-N	
----------	--	---------------------------------------	------------------------	---	-------------------------------------	-----	-----	-------------------	--------------------	----------------	-----------	------	--

	1											
CuE		2983, 2906	1598, 1538	141 7	1288, 1369		1178	-	868, 778		49 0	
CuECl	3090	2983	1600, 1530	141 4	1360, 1310		1181 , 1138	-	863, 791, 767	668	57 7	
CuEbpy	3060, 3044	2977	1644, 1515	140 7	1361	127 5, 123 2	1169 , 1060	-	864, 820, 779		50 9, 57 8	422, 448
CuEClbpy	3068, 3047	2979	1654,16 10,1551	147 2,14 19	1364	127 0 ,12 16	1090 , 1050	-	795, 759	642	57 5,5 15	463
CuEC ₁ V ⁺ . PF ₆	3056, 3129	2979, 2932	1650, 1618, 1574	149 9,14 46	1383	122	1157 , 1078	846	741	-	55 8	483
CuEClC ₁ V ⁺ .PF ₆	3098, 3029	2999, 2881, 2848	1716,16 39,1615, 1548	149 8,14 19	1347	122 3	1193 , 1088	829	716	669	55 9	482

Both CuECl and its adducts, CuEbpy and CuEClbpy, CuEC₁V⁺.PF₆⁻ and CuEClC₁V⁺.PF₆⁻, exhibit single bands at 3098, 3044, and 3043, 3056 and 3029 cm⁻¹ correspondingly. The bands correspond to aromatic and olefinic C-H stretching vibrations, indicating successful coordination with bipyridine [8,9]. The metal complexes show aliphatic C-H stretching bands at 2983 cm⁻¹ for both CuECl and CuE, and at 2977 cm⁻¹, 2982 cm⁻¹ for CuEClbpy and CuEbpy, 2979 cm⁻¹, 2932 cm⁻¹ of CuEC₁V⁺.PF₆⁻, 2999, 2881 and 2848cm⁻¹ of CuEClC₁V⁺.PF₆⁻ respectively [10]. Characteristic bands appear at 1600 cm⁻¹, 1530 cm⁻¹ for CuECl; 1602 cm⁻¹, 1532 cm⁻¹ for CuClbpy; 1598 cm⁻¹, 1538 cm⁻¹ for CuE; and 1644 cm⁻¹, 1515 cm⁻¹ for CuEbpy, 1650, 1618 and 1574 cm⁻¹ for CuEC₁V⁺.PF₆⁻, 1716,1639,1615 and 1548 cm⁻¹ for CuEClC₁V⁺.PF₆⁻. These are associated with C=C stretching and C=O vibrations. The corresponding bending vibrations are observed at 1417 cm⁻¹ for CuE, 1414 cm⁻¹ for CuECl, 1415 cm⁻¹ and 1407 cm⁻¹ for CuEbpy, 1499, 1446,1416 cm⁻¹ for CuEC₁V⁺.PF₆⁻ and 1498, 1419 cm⁻¹ for CuEClC₁V⁺.PF₆^{-[11]}. Bending vibrations are also observed at 1360 cm⁻¹, 1310 cm⁻¹ for CuECl, 1288 cm⁻¹, 1369 cm⁻¹ for CuE, 1361 cm⁻¹ for CuEbpy, 1316 cm⁻¹ for CuEClbpy, 1383 cm⁻¹ for CuEC₁V⁺.PF₆, 1347 cm⁻¹ for CuEClC₁V⁺.PF₆^{-[11]}. Pronounced bands appear for CuEbpy at 1218 cm⁻¹, and for CuEClbpy at 1275 cm⁻¹, 1232 cm⁻¹, 1222 cm⁻¹ for CuEC₁V⁺.PF₆⁻, 1223 cm⁻¹ for CuEClC₁V⁺.PF₆^{-[11]}. Bending vibrations appear at 1181 cm⁻¹, 1138 cm⁻¹ for CuECl, 1288 cm⁻¹ for CuE, 1169 cm⁻¹, 1060 cm⁻¹ for CuEbpy, and 1083 cm⁻¹, 1016 cm⁻¹ for CuEClbpy, 1157, 1078 cm⁻¹ for CuEC₁V⁺.PF₆⁻ and 1193, 1088 cm⁻¹ for CuEClC₁V⁺.PF₆⁻. Bands at 863 cm⁻¹, 791 cm⁻¹, 767 cm⁻¹ appear in CuECl, while 868 cm⁻¹, 778 cm⁻¹ are seen for CuE, and 684 cm⁻¹, 820 cm⁻¹, 779 cm⁻¹ for CuEbpy, 851 cm⁻¹, 725 cm⁻¹ for CuEClbpy. Adduct compounds appear bands at 846 cm⁻¹ for CuEC₁V⁺.PF₆, 829 cm⁻¹ for CuEClC₁V⁺.PF₆, these bands are assigned to vibrational modes involving bending coupled with stretching within the PF₆ anion. Addition to appear bands at 741 cm ¹ for CuEC₁V⁺.PF₆⁻, 716 cm⁻¹ for CuEClC₁V⁺.PF₆⁻, included out of plane stretching C-C ^[12]. C–Cl stretching bands appear at 668 cm⁻¹ for CuECl and 645 cm⁻¹, 607 cm⁻¹ for CuEClbpy, 606 cm⁻¹ for CuEC₁V⁺.PF₆⁻, 669 cm⁻¹ for CuEClC₁V⁺.PF₆⁻ [13]. Cu–O stretching appears at 577 cm⁻¹ CuECl, 641 cm⁻¹ CuE, 637 cm⁻¹, 609 cm⁻¹ CuEbpy and 507 cm⁻¹ CuEClbpy, 558 sharp cm⁻¹ for CuEC₁V⁺.PF₆⁻, 559 cm⁻¹ for CuEClC₁V⁺.PF₆⁻. Finally, adduct bands attributed to Cu–N bending vibrations are observed at 509 cm⁻¹ CuEbpy, 474 cm⁻¹ CuEClbpy, 483 cm⁻¹ very sharp for CuEC₁V⁺.PF₆, 482 cm⁻¹ for CuEClC₁V⁺.PF₆. the presence of these bands, not observed in the precursor complexes, is assigned to Cu-N bending vibrations, further confirming coordination with bipyridine and $C_1V^+.PF_6^-$ at the same time, we note the absence of the appearance of bands in the complexes CuE and CuECl, which indicates the formation of new complexes which it are adducts complexes [12-14].

Mass spectroscopy of Cu²⁺ complexes

LC- mass spectrum of CuE, CuECl, CuEbpy, CuEClbpy, CuEC $_1V^+$.PF $_6^-$ and CuEClC $_1V^+$.PF $_6^-$ are depicted in figures 2 to 7.

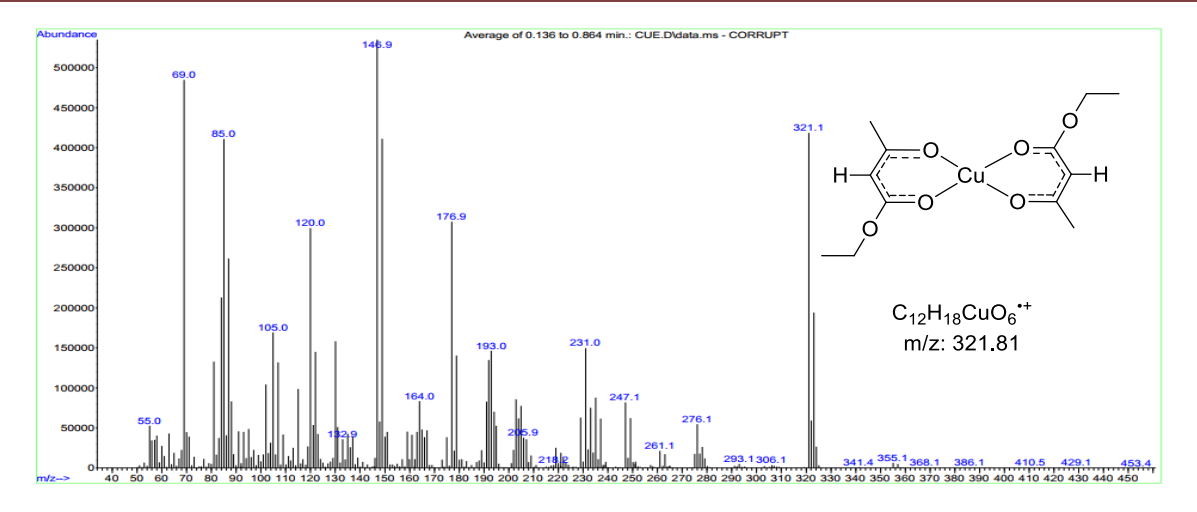


Figure 2: LC- mass spectrum of CuE complex.

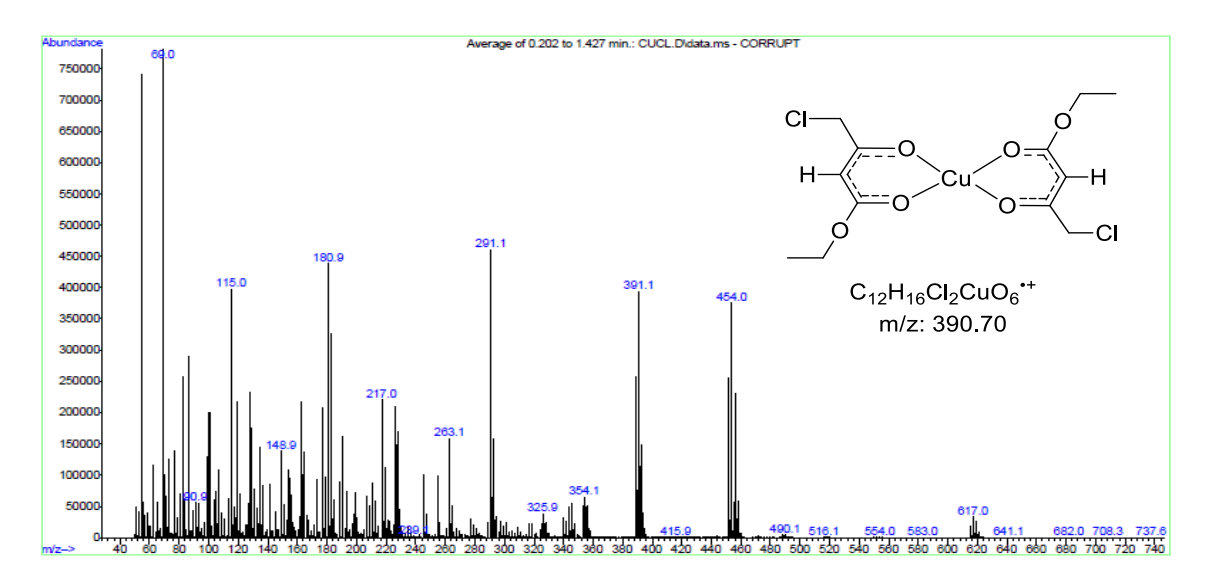


Figure 3: LC- mass spectrum of CuECl complex.

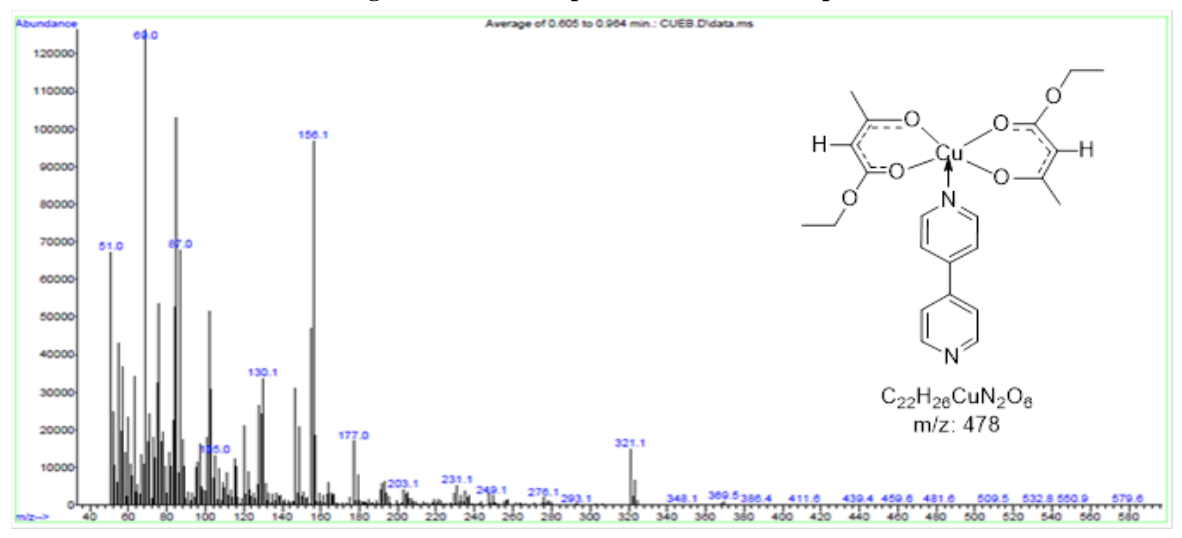


Figure 4: LC- mass spectrum of CuEbpy complex.

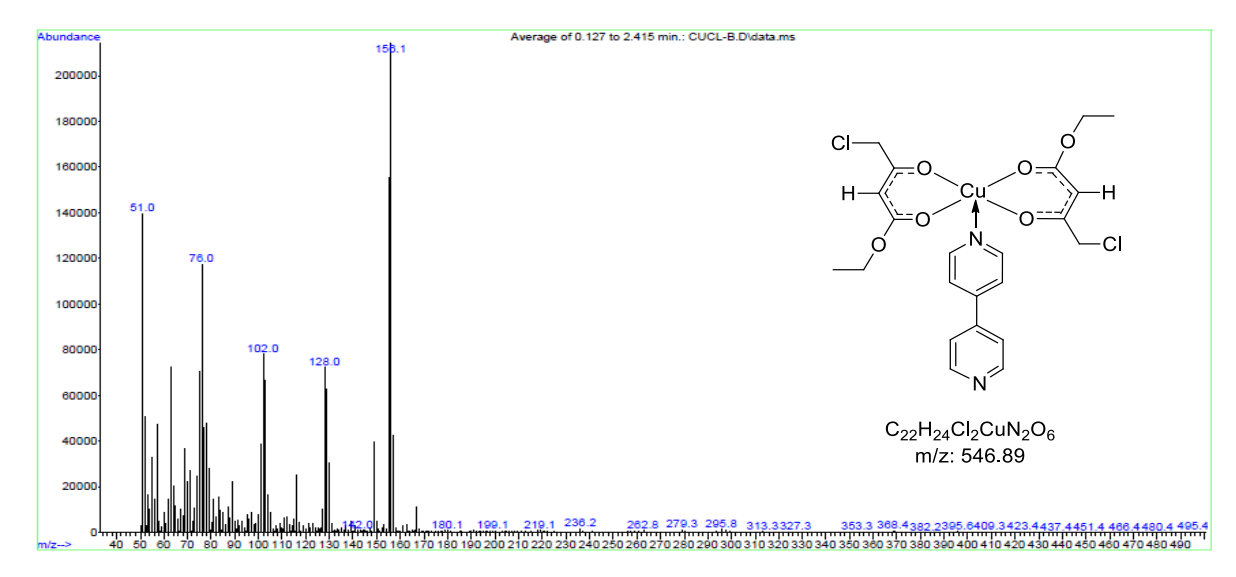


Figure 5: LC- mass spectrum of CuEClbpy complex.

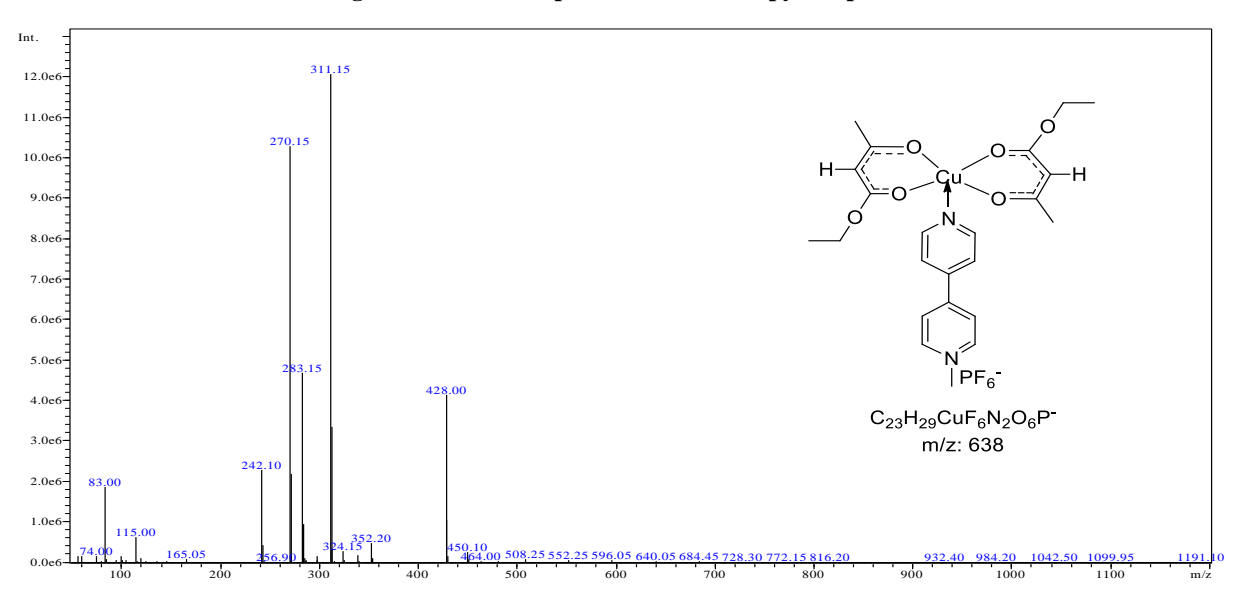


Figure 6: LC- mass spectrum of CuEC₁V⁺.PF₆⁻ complex.

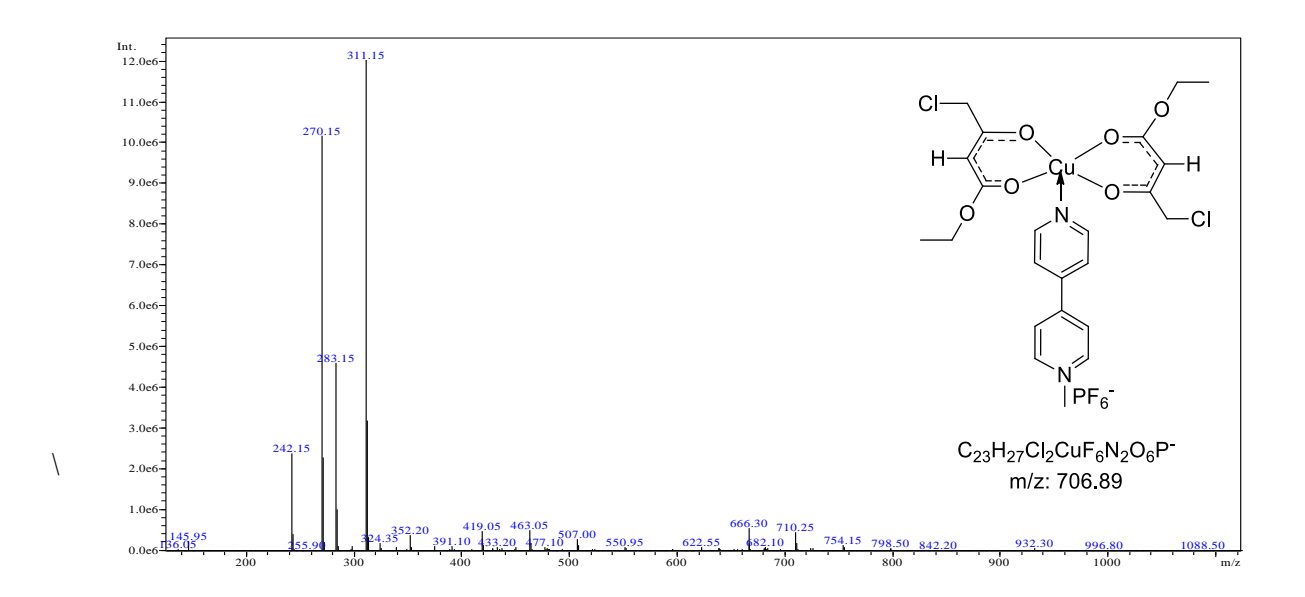


Figure 7: LC- mass spectrum of CuEClC₁V⁺.PF₆ complex.

Figure 2 represent the LC- mass spectra of CuE complex appear peak at m / z = 321.1 due to the molecular ion. The show peak at m/z= 261.1 suggests which confirm the structure $[C_{10}H_{14}CuO_4]^+$. The spectra show peaks at m/z= 456.46, 429.45, 411.40 , 369.32, 355.29, 341.31, 322.82, 276.1, 247, 231, 205.9, 193, 176.9 and 164 due to $[C_{16}H_{25}Cu_2O_7]^+$, $[C_{15}H_{26}Cu_2O_6]^+$, $[C_{14}H_{20}Cu_2O_6]^+$, $[C_{14}H_{20}Cu_2O_6]^+$, $[C_{14}H_{20}Cu_2O_6]^+$, $[C_{15}H_{15}Cu_2O_6]^+$, $[C_{1$

 $\begin{array}{ll} [C_{11}H_{14}Cu_2O_6]^+, [C_{10}H_{12}Cu_2O_6]^+, [C_{10}H_{14}Cu_2O_5]^+, [C_{12}H19CuO_6]^+, [C_{11}H_{17}CuO_4]^+, [C_{10}H_{15}CuO_3]^+, [C_8H_8CuO_4]^+, [C_6H_9CuO_3]^+, [C_6H_9CuO_2]^+ \ and \ [C_4H_5CuO_3]^+ \ respectively \\ \end{array} \\ \begin{array}{ll} [C_1H_{17}CuO_4]^+, [C_1H_{17}CuO_4$

Figure 3 represent the LC- mass spectra of CuECl complex appear peak at m / z = 391.1 due to the molecular ion. The show peak at at m / z = 391.1 suggests of Cl atom and which confirm the structure [$C_{12}H_{16}ClCuO_{5}$]⁺. The spectrum showed peaks at m/z= 710.54, 732.94, 682.49, 618.84, 582.42, 552.39, 515.50, 487.45, 457.42, 453.48, 291.1, 263.1, 217, 180.9, 148.9, 115.1 and 90.9 due to [$C_{25}H_{36}C_{12}Cu_{2}O_{11}$]⁺,[$C_{23}H_{31}C_{13}Cu_{2}O_{12}$]⁺, [$C_{23}H_{32}C_{12}Cu_{2}O_{11}$]⁺, [$C_{18}H_{25}C_{13}Cu_{2}O_{9}$]⁺, [$C_{19}H_{28}C_{12}Cu_{2}O_{8}$]⁺, [$C_{18}H_{26}C_{12}Cu_{2}O_{7}$]⁺, [$C_{18}H_{26}Cu_{2}O_{9}$]⁺, [$C_{16}H_{24}Cu_{2}O_{9}$]⁺, [$C_{15}H_{22}Cu_{2}O_{8}$]⁺, [$C_{17}H_{26}Cu_{2}O_{6}$]⁺, [$C_{11}H_{16}CuO_{5}$]⁺, [$C_{9}H_{12}CuO_{5}$]⁺, [$C_{8}H_{10}CuO_{3}$]⁺, [$C_{4}H_{5}CuO_{4}$]⁺, [$C_{6}H_{11}O_{2}$]⁺, [$C_{4}H_{7}Cl$]⁺ and [$C_{4}H_{5}O$]⁺ respectively. The intensive peak (base peak) at m/z= 69 was attributed to [$C_{4}H_{5}O$]⁺ [I_{15-17}].

Figure 4 represent the redrawing and original LC- mass spectrum of CuEbpy complex. The spectra showed a peak at range m / z = 509.5 - 532.8 because to the mother ion . The spectrum showed an peak about m / z = 321.1 due to $[C_{12}H_{18}CuO_6]^{+}$ [21]. The intensive peak (base peak) at m/z= 156.1 and 69 was attributed to $[C_{10}H_8N_2]^{+}$ and $[C_4H_5O]^{+}$. The spectrum showed peaks at m/z= 578.08, 554.07, 532.05, 510.47, 479.56, 452.05, 439.95, 411.90, 386.89 , 371.92, 369.88, 350.86, 231.01, 177, 130, 87.04, 53.03 and 51.07 due to $[C_{28}H_{26}CuN_4O_6]^{+}$, $[C_{27}H_{28}CuN_3O_6]^{+}$, $[C_{27}H_{24}CuN_4O_4]^{+}$, $[C_{29}H_{29}Cu_2N_2O_6]^{+}$, $[C_{22}H_{28}Cu_2N_2O_2]^{+}$, $[C_{25}H_{28}CuN_2O_2]^{+}$, $[C_{19}H_{24}CuN_2O_6]^{+}$, $[C_{17}H_{20}CuN_2O_6]^{+}$, $[C_{16}H_{21}CuNO_6]^{+}$, $[C_{19}H_{20}CuN_2O_2]^{+}$, $[C_{16}H_{20}CuNO_5]^{+}$, $[C_{16}H_{17}CuNO_4]^{+}$,

 $[C_{12}H_{18}CuO_4]^+$, $[C_5H_6CuO_3]^+$, $[C_9H_8N]^+$, $[C_4H_7O_2]^+$, $[C_3H_3N]^+$ and $[C_4H_3]^+$ respectively [15-17].

Figure 5 represent the redrawing and original LC- mass spectrum of CuEClbpy complex. The appear of peak at m / z = 128.17 suggests which confirm the structure $[C_7H_{12}O_2]^+$. The intensive peak (base peak) at m / z = 156.18 was attributed to $[C_{10}H_8N_2]^+$. The spectrum showed peaks at m / z = 467.01, 451.40, 435.92, 481.04, 393.28, 383.91, 368.87, 350.86, 326.84, 314.78, 235.75, 295.80, 279.73,260.73, 219.68 ,179.62, 102, 76.98, 53.03 and 51.07 due to $[C_{22}H_{29}CuNO_6]^+$, $[C_{21}H_{22}ClCuNO_4]^+$, $[C_{19}H_{20}CuN_2O_6]^+$, $[C_{23}H_{31}CuNO_6]^+$, $[C_{14}H_{16}ClCuNO_6]^+$, $[C_{17}H_{22}CuNO_5]^+$, $[C_{16}H_{17}CuNO_4]^+$, $[C_{14}H_{17}CuNO_4]^+$, $[C_{15}H_{12}ClO_3]^+$, $[C_{15}H_{12}ClO_3]^+$, $[C_{15}H_{12}ClO_3]^+$, $[C_{15}H_{17}CuNO_4]^+$, $[C_{15}H_{17}CuNO_4]^+$, $[C_{15}H_{12}CuNO_5]^+$, $[C_{15}H_{17}CuNO_4]^+$, $[C_{15}H_{17}CuN$

Figure 6 represent the redrawing and original LC- mass spectrum of $CuEC_1V^+.PF_6^-$ complex appear a peak at m / z = 640.05 because to the mother ion. Four high-intensity peaks appeared in the spectra at m / z = 242, 270, 311 and 428 back to $[M^{*+} - C_9H_{12}CuO_4^+]^+$, $[M^{*+} - C_{10}H_{15}CuO_5^{7*}]^+$, $[M^{*+} - C_{14}H_{18}CuNO_3^{2*}]^+$ and $[M^{*+} - C_{19}H_{27}CuNO_6^+]^+$ respectively. The spectrum showed peaks at m/z = 74, 114 and 164 due to $[M^{*+} - C_3H_6O_2^{2+}]^+$, $[M^{*+} - C_6H_{10}O_2^+]^+$ and $[M^{*+} - C_4H_5CuO_3^+]^+$ respectively $[^{8]}$. The intensive peak (base peak) at m/z = 508, 594, 684, 772, 937, 1099 and 1193 was attributed to $[C_{20}H_{19}Cu_2N_2O_6]^+$, $[C_{25}H_{31}Cu_2N_2O_6]^+$, $[C_{30}H_{41}Cu_2N_2O_6]^+$, $[C_{36}H_{44}Cu_2N_3O_8]^+$, $[C_{45}H_{53}Cu_2N_3O_{11}]^+$, $[C_{56}H_{67}Cu_2N_3O_{12}]^+$ and $[C_{57}H_{72}Cu_3N_4O_{12}]^+$ respectively $[^{15-17}]$.

Figure 7 represent the redrawing and original LC- mass spectrum of $CuEClC_1V^+.PF_6^-$ complex appear peak at m / z = 640.05 because to the mother ion. One high-intensity peaks appeared in the spectra at m / z = 283 back to $[M^{\bullet+}-C_{11}H_{24}CuO_4^+]^+$. The spectra showed peaks at m/z = 134, 325, 350, 390, 420, 464, 506, 551, 623, 667 and 750 due to $[M^{\bullet+}-C_3H_3CuO_2^+]^+$, $[M^{\bullet+}-C_1H_{16}CuNO_4^+]^+$, $[M^{\bullet+}-C_1H_{15}CuN_2O_4^+]^+$, $[M^{\bullet+}-C_1H_{19}CuN_2O_4^+]^+$, $[M^{\bullet+}-C_1H_{19}CuN_2O_4^+]^+$, $[M^{\bullet+}-C_2H_{19}CuNO_4^+]^+$, $[M^{\bullet+}-C_2H_{19}CuNO_4^+]^+$, $[M^{\bullet+}-C_2H_{19}CuNO_4^+]^+$, $[M^{\bullet+}-C_2H_{19}CuNO_4^+]^+$, $[M^{\bullet+}-C_2H_{19}CuNO_4^+]^+$, $[C_2H_{19}CuNO_4^+]^+$, $[C_2H_{19}CuNO_$

X-Ray Diffraction analysis of Cu²⁺ complexes and their adducts

The XRD pattern of Cu²⁺ complexes are presented in figures 8. The XRD data of the complexes are listed in tables 2.

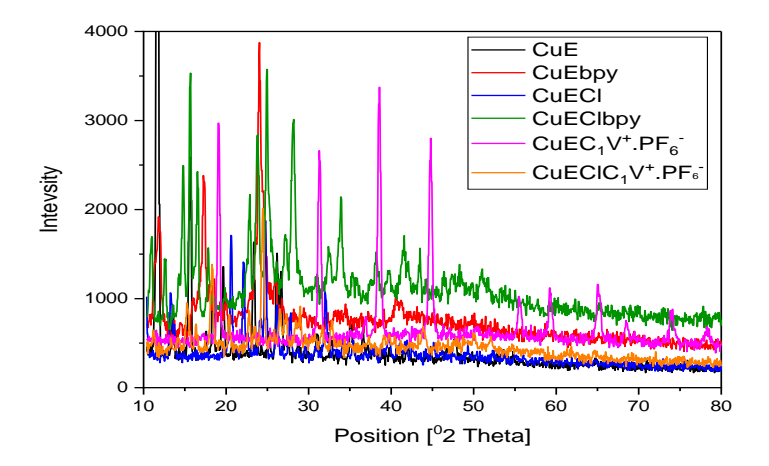


Figure 8: The XRD pattern of CuE, CuEbpy and CuEClbpy, CuEC₁V⁺.PF₆⁻ and CuEClC₁V⁺.PF₆⁻ complex The largest peak at 11.8° , 24.7° , 24° , 25° , 38.5° and 24.3° for CuE, CuEbpy, CuEClbpy, CuEClbp

$$D = \frac{\kappa\lambda}{\beta} * \frac{1}{\cos\theta}$$
 Eq.1

Table 2: Williamson-Hall model for show values of strain and crystallite sizes.

CuE		CuECl		CuEbpy		CuEClbpy	y
Slope = strain, ε	Crystal size L = Kλ/Intercep t	Slope = strain, ε	Crystal size $L = K\lambda/Intercept$	Slope = strain, ε	Crystal size L = Kλ/Interce pt	Slope = strain, ε	Crystal size L = K⅓Intercept
- 0.00158	40.2936	3.4597	58.8906774	0.00712	31.899116	0.00282	59.9316742

Table 3: Strain and crystallite sizes of CuEC₁V⁺.PF₆ and CuEClC₁V⁺.PF₆ according to Williamson-Hall model.

CuEC ₁ V ⁺ .PF ₆ ⁻		CuEClC ₁ V ⁺ .PF ₆ ⁻	
Slope= strain, ε	Crystal size L= Kλ/Intercept	Slope= strain, ε	Crystal size L= Kλ/Intercept
-0.01368	7.057074933	0.03239	24.85124921

The Scherrer equation represents a basic approach that considers solely the physical broadening, neglecting contributions from instrumental effects. In contrast, the Williamson–Hall method addresses this limitation $^{[21-24]}$.

$$\beta \cos \theta = K \lambda D + 4 \varepsilon \sin \theta$$
 Eq. 2

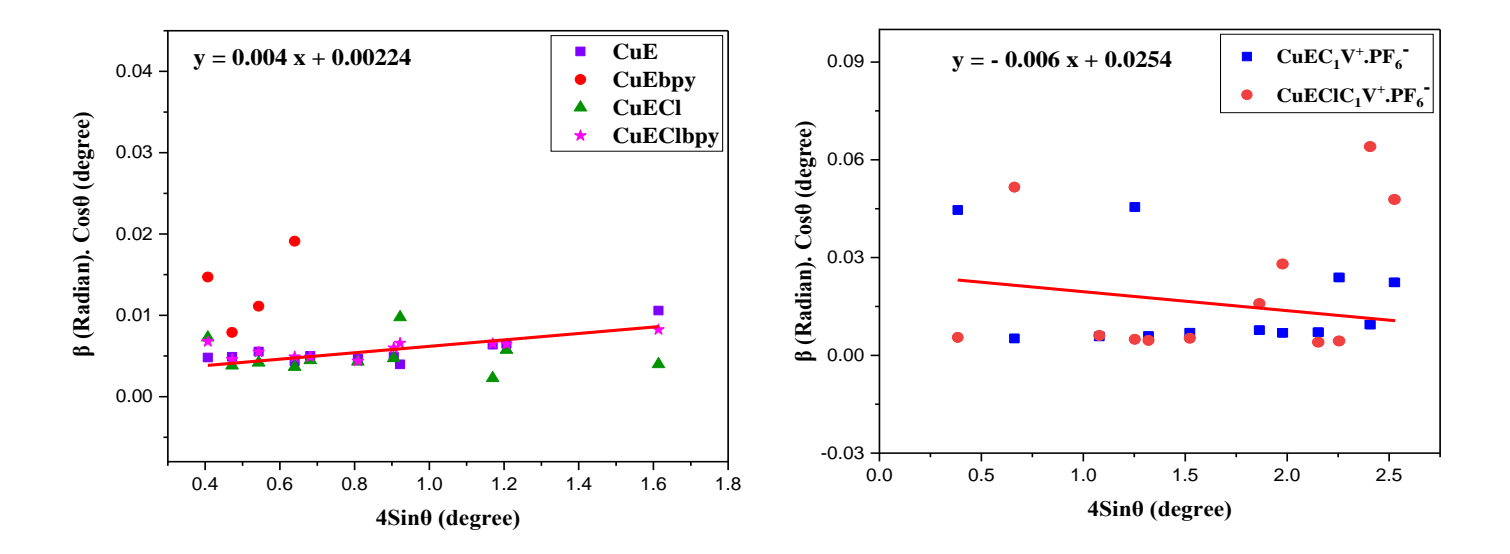
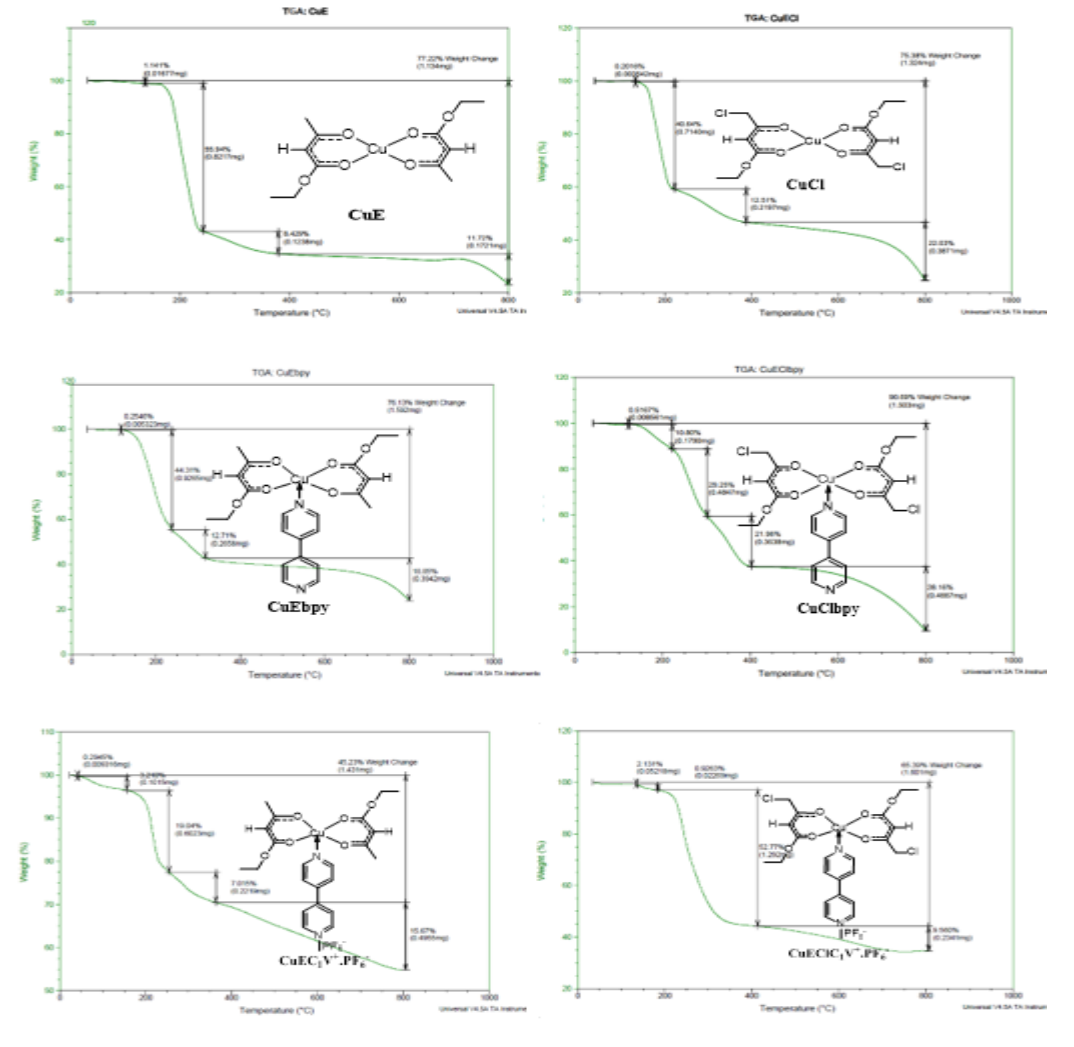


Figure 9: Plot of compounds : CuE and CuECl, CuEbpy, CuEClbpy, CuEC $_1V^+$.PF $_6$ and CuEClC $_1V^+$.PF $_6$. Thermo gravimetric analyses of copper complexes

The copper (II) complexes put their were analyzed by thermo gravimetric analyses TGA to 800° C of symblos CuE, CuECl, CuEbpy, CuEClbpy, CuEClV⁺.PF₆⁻ and CuEClC₁V⁺.PF₆⁻ heating to 80 ml / min in under Ar. The TGA curves are depicted in figure 10. The data are presented in table 4 [25, 26].



 Cu^{2+} complexes.

Table 4: Thermogravimetric analyses data of Cu²⁺complexes.

Complexes	Temperature	Ü	t loss %	Decomposition	Liberated part
M.wt (g.mol ⁻¹)	range (⁰ C)	(Molecular	weight loss,	product	Liberated part
W.W. (g.mor)	runge (C)	g.mol ⁻¹)	weight 1055,	product	
		Found	Calculated		
CuE	36.26 – 170.32	1.141	1.01	H.	C ₁₂ H ₁₇ CuO ₆ *
321.1 g.mol ⁻¹	170.32 – 257.29	55.94	56.06	C ₄ H ₈	$C_{10}H_{10}CuO_6$
	257.29 – 429.89	8.429	9.0	CuE	1/2H ₂ O
	429.89 – 799.92	11.72	15	*CH ₃	C ₁₂ H ₁₈ CuO ₆ •
CuECl	37.76 - 146.62	0.2016	1.01	H.	$C_{12}H_{15}Cl_2CuO_6$
390.1 g.mol ⁻¹	146.62 - 224.64	40.64	42.08	C ₃ H ₆	C ₁₁ H ₁₉ ClCuO ₆
	224.64 – 427.31	12.51	15	*CH ₃	C ₁₁ H ₁₃ Cl ₂ CuO ₆
	427.31 – 800.59	22.03	18	H ₂ O	CuECl
CuEbpy 521.09 g.mol ⁻¹	48.85 – 134.23	0.2546	1.01	Н.	C ₂₂ H ₂₅ CuN ₂ O ₆ *
	134.23 – 239.68	44.31	45.03	C ₂ H ₅ O*	C ₂₀ H ₂₁ CuN ₂ O ₅ *
	239.68 – 329.04	12.71	14.02	CH ₂ 2•	C ₂₁ H ₂₅ CuN ₂ O ₆ *
	329.04 – 800.71	18.85	18.0	H ₂ O	CuEbpy
	44.68 – 143.9	0.5167	1.01	H.	C ₂₂ H ₂₃ Cl ₂ CuN ₂ O ₆ *
CuEClbpy 560.05 g.mol ⁻¹	143.9 – 226.31	10.80	9.0	CuEClbpy	1/2H ₂ O
	226.31 – 303.72	29.25	29.04	C ₂ H ₅	C ₂₀ H ₁₉ Cl ₂ CuN ₂ O ₆ *
	303.72 – 478.78	21.96	18	H ₂ O	CuEClbpy
	478.78 – 800.41	28.16	27.01	CHN ₂ ·	C ₂₁ H ₂₃ Cl ₂ CuNO ₆
	23.67 – 65.6	0.2945	1.01	Н.	C ₂₃ H ₂₈ CuF ₆ N ₂ O ₆ P*
CuEC ₁ V ⁺ . PF ₆	65.6 – 171.85	3.210	2.02	H2 ² *	$C_{23}H_{29}CuF_6N_2O_6P$
638 g.mol ⁻¹	171.85- 260.14	19.04	18	CuEC ₁ V ⁺ .PF ₆	H ₂ O
	260.14– 378.27	7.015	9.0	CuEC ₁ V ⁺ .PF ₆	1/2H ₂ O
	378.27 – 805.37	15.67	15.02	*CH ₃	C ₂₂ H ₂₆ CuF ₆ N ₂ O ₆ P*

	34.63 182.15	-	2.131	2.02	H ₂ ² •	C ₂₃ H ₂₅ Cl ₂ CuF ₆ N ₂ O ₆ P ²
CuEClC ₁ V ⁺ .PF ₆	182.15 205.43	1	0.9263	1.01	Н.	C ₂₃ H ₂₆ Cl ₂ CuF ₆ N ₂ O ₆ P*
706.89 g.mol ⁻¹	205.43 424.18	1	52.77	53.03	C ₃ H ₃ N ² •	C ₂₀ H ₂₆ Cl ₂ CuF ₆ NO ₆ P
	424.18 806.53	_	9.560	9.0	CuEClC ₁ V ⁺ .	1/2H ₂ O

The TG curves were drawn as temperature T °C with wt loss %. Decomposition pattern of Cu²⁺ occur in four step for CuE, four step for CuECl, four steps for CuEbpy, five steps for CuEClbpy of weight losses as shown in figure 8 respectively. Complex of CuE in first phase at 140- 240 °C temperature 0.8217 mg weight loss with 55.94 %, returning to $C_5H_8CuO_4$ molecule and liberated part from complex is $C_9H_{14}CuO_2$, second phase at 240 - 378 °C temperature 0.1238 mg weight loss with 8.429 %, returning to C₂H₄ molecule and liberated part from complex is C₁₂H₁₈CuO₆, third phase at 378 - 800 °C temperature 0.1721 mg weight loss with 11.72 %, returning to C₃H₆ molecule and liberated part from complex is C₁₁H₁₆CuO₆. Complex of CuECl in first phase at 137.5- 225 °C temperature 0.7140 mg weight loss with 40.64 %, returning to C₆H₁₀CuO molecule and liberated part from complex is C₆H₆Cl₂O₅, second phase at 225 – 387.5 °C temperature 0.2197 mg weight loss with 12.51 %, returning to C₂H₄O molecule and liberated part from complex is C₁₀H₁₂Cl₂CuO₅, third phase at 387.5 – 800 °C temperature 0.3871 mg weight loss with 22.03 %, returning to C₄H₇O₂ molecule and liberated part from complex is C₈H₉Cl₂CuO₄. It is noted for the thermal decomposition of both complexes CuECl is more stable than CuE. Complex of CuEbpy in first phase at 125 - 245 °C temperature 0.9265 mg weight loss with 44.31 %, returning to $C_8H_{10}CuO_4$ molecule and liberated part from complex is $C_{17}H_{22}O_2$, second phase at 245 – 320 °C temperature 0.2658 mg weight loss with 12.71 %, returning to C₄H₅O molecule and liberated part from complex is $C_{21}H_{28}CuO_5$, third phase at 320 – 800 °C temperature 0.3942 mg weight loss with 18.85 %, returning to C_7H_{12} molecule and liberated part from complex is C₁₈H₂₁CuO₆ [27]. Complex of CuEClbpy in first phase at 125 - 225 °C temperature 0.1790 mg weight loss with 10.80 %, returning to C₃H₅O molecule and liberated part from complex is C₂₀H₂₂Cl₂CuN₂O₅, second phase at 225 – 300 °C temperature 0.4847 mg weight loss with 29.25 %, returning to C₄H₆CuNO₂ molecule and liberated part from complex is $C_{19}H_{21}Cl_2NO_4$, third phase at $300-400\,^{\circ}C$ temperature 0.3638 mg weight loss with 21.96 %, returning to C₉H₁₆ molecule and liberated part from complex is C₂₄H₁₁Cl₂CuN₂O₆ and fourth phase at 400 – 800 °C temperature 0.4667 mg weight loss with 28.16 %, returning to C₁₀H₈N₂ molecule and liberated part from complex is $C_{13}H_{19}Cl_2CuO_6$ [27]. It is noted for the thermal decomposition of both complexes CuEClbpy is more stable than CuEbpy. Returning to H₂² molecule and liberated part from complex is C₂₃H₂₇CuF₆N₂O₆P², third phase at 171.85 – 260.14 °C temperature 0.6023 mg weight loss with 19.04 %, returning to H₂O molecule and liberated part from complex is C₂₃H₂₉CuF₆N₂O₆P⁻, fourth phase at 260.14 – 378.27 °C temperature 0.2219 mg weight loss with 7.015 %, returning to 1/2H₂O molecule and liberated part from complex is C₂₃H₂₉CuF₆N₂O₆P and fifth phase at 378.27 – 805.37 °C temperature 0.4955 mg weight loss with 15.67 %, returning to 'CH₃ molecule and liberated part from complex is C₂₂H₂₆CuF₆N₂O₆P'. Complex of CuEC₁V⁺.PF₆⁻ in first phase at 23.67 – 65.6 °C temperature 0.009316 mg weight loss with 0.2945 %, returning to H* molecule and liberated part from complex is C₂₃H₂₈CuF₆N₂O₆P*, second phase at 65.6 – 171.85 °C temperature 0.1015 mg weight loss with 3.210 %, returning to H₂²* molecule and liberated part from complex is C₂₃H₂₇CuF₆N₂O₆P²*, third phase at 171.85 - 260.14 °C temperature 0.6023 mg weight loss with 19.04 %, returning to H₂O molecule and liberated part from complex is C₂₃H₂₉CuF₆N₂O₆P, fourth phase at 260.14 – 378.27 °C temperature 0.2219 mg weight loss with 7.015 %, returning to 1/2H₂O molecule and liberated part from complex is C₂₃H₂₉CuF₆N₂O₆P and fifth phase at 378.27 – 805.37 °C temperature 0.4955 mg weight loss with 15.67 %, returning to 'CH₃ molecule and liberated part from complex is $C_{22}H_{26}CuF_6N_2O_6P^{\bullet}[28-31]$.

Complex of $CuEClC_1V^+.PF_6^-$ in first phase at 34.63-182.15 °C temperature 0.05218 mg weight loss with 2.131 %, returning to $H_2^{2^*}$ molecule and liberated part from complex is $C_{23}H_{25}Cl_2F_6N_2O_6P^-$, second phase at 182.15-205.43 °C temperature 0.02269 mg weight loss with 0.9263 %, returning to H* molecule and liberated part from complex is $C_{23}H_{25}Cl_2F_6N_2O_6P^-$, third phase at 205.43-424.18 °C temperature 1.292 mg weight loss with 52.77 %, returning to $C_3H_3N^{2^*}$ molecule and liberated part from complex is $C_{20}H_{24}Cl_2F_6NO_6P^-$ and fourth phase at 424.18-806.53 °C temperature 0.2341 mg weight loss with 9.560 %, returning to $1/2H_2O$ molecule and liberated part from complex is $C_{23}H_{27}Cl_2F_6N_2O_6P^-$ [28-31]. It is noted for the thermal decomposition of both complexes $CuEClC_1V^+$. PF_6^- is more stable than $CuEC_1V^+$. PF_6^- . The order of thermal stability of complexes was:

 $CuEClC_1V^+.PF_6^->CuEC_1V^+.PF_6^->CuEbpy>CuECl>CuEClbpy>CuE.$

3.1.5. Energy Dispersive X-ray spectroscopy of Cu (II) complexes (EDX)

The morphology and structure formation elemental composition characteristics of cu2+ complexes were elucidated by EDX analysis. The EDX spectra of CuE, CuEbpy, CuEClbpy, CuEClc1V+.PF6- and CuEC1V+.PF6- are shown in Figures 11. EDX analysis revealed the presence of Cu (II) in all compounds that support the formation of copper

complexes. Also, the presence of (N) atom confirms the content of the Cu-N, i.e. the formation of adduct complex from its precursor copper complex

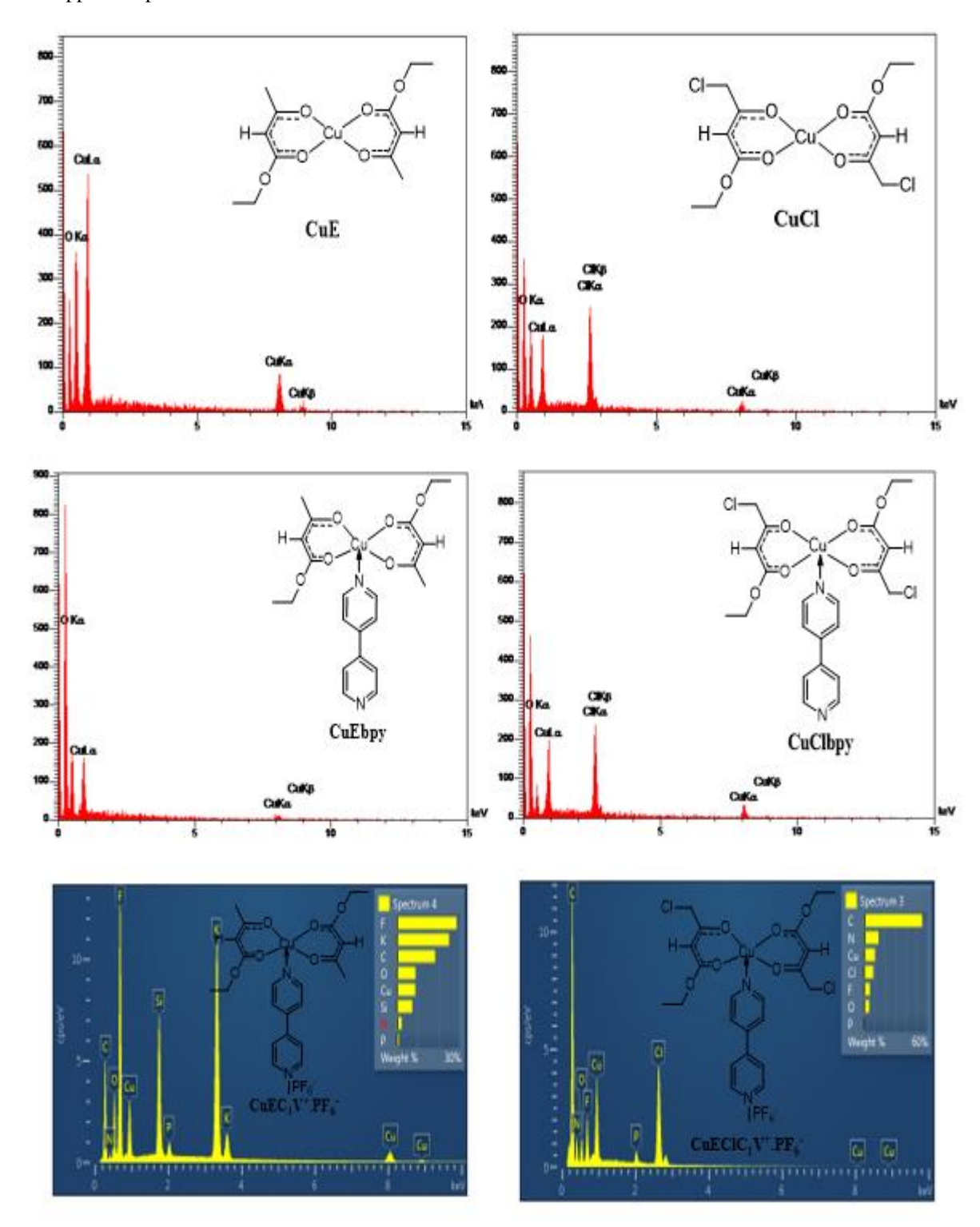


Figure 11: EDX spectrum of the CuE, CuECl, CuEbpy, CuEClbpy, CuEC $_1V^+$.PF $_6^-$ and CuEClC $_1V^+$.PF $_6^-$ complex.

From the EDX spectral analysis revealed that the copper (II) with ethyl 4-chloro acetoacetate and ethyl acetoacetate ligands and the formation of complexes CuE and CuECl and the formation of a homogeneous form. Figures 11 shows peaks of elements present in the complexes formed in each of complexes CuE and CuEbpy It shows strong peaks of O, N, C, and Cu while in complexes CuECl and CuEClbpy it shows peaks of both O, N, C, Cu and Cl. The complexes $CuEC_1V^+.PF_6^-$ it shows strong peaks of C, N, O, Cu, F, P and Cl [32]

3.1.6. Ultraviolet -visible Absorption Spectroscopy of Cu 2+ complexes

Ultraviolet -visible Absorption Spectroscopy of the ligands E and ECl and their Cu (II) Complexes were record in different solvents (C₆H₆, DCM, acetone, EtOAc, MeCN, EtOH, MeOH, DMF, DMSO and H₂O). The spectra were recorded at low and high concentrations.

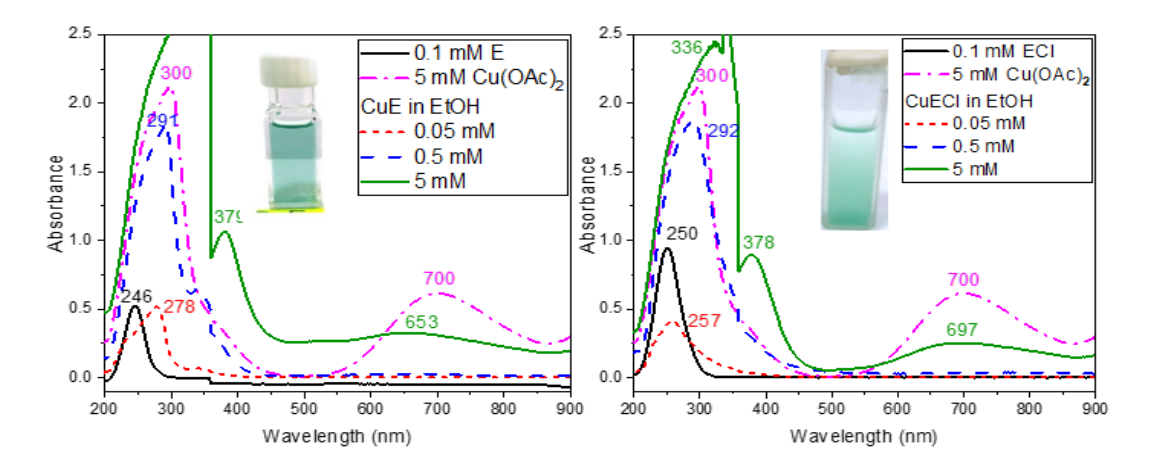


Figure 12: Absorption spectrum of 0.1 mM (black) of ethyl acetoacetate, 5 mM (purple) of copper acetate, 0.05 mM (red), 0.5 mM (blue) and 5 mM (green) of **CuE** complex in EtOH.

Figure 13: Absorption spectrum of 0.1 mM (black) of ethyl acetoacetate, 5 mM (purple) of copper acetate, 0.05 mM (red), 0.5 mM (blue) and 5 mM (green) of **CuECl** complex in EtOH.

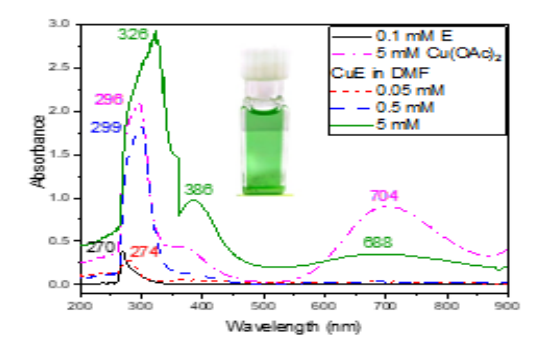


Figure 14: Absorption spectrum of 0.1 mM (black) of ethyl acetoacetate, 5 mM (purple) of copper acetate, 0.05 mM (red), 0.5 mM (blue) and 5 mM (green) of CuE complex in DMF.

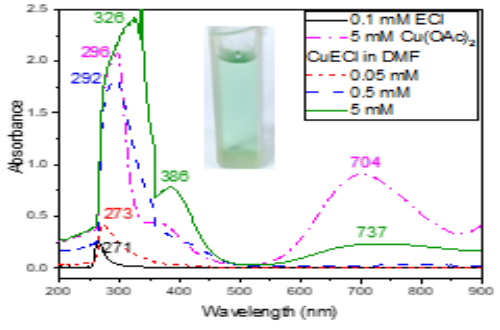


Figure 15: Absorption spectrum of 0.1 mM (black) of ethyl4-chloro acetoacetate, 5 mM (purple) of copper acetate, 0.05 mM (red), 0.5 mM (blue) and 5 mM (green) of CuECl complex in DMF

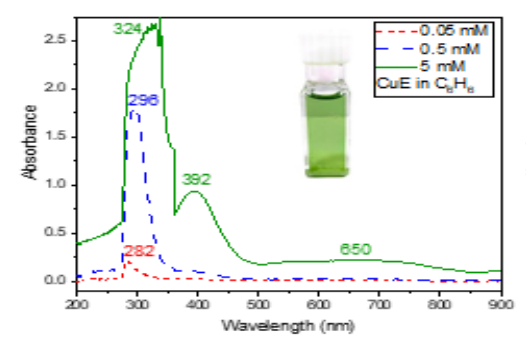


Figure 16: Absorption spectrum of 0.05 mM (red), 0.5 mM (blue) and 5 mM (green) of CuE complex in C_cH_6 .

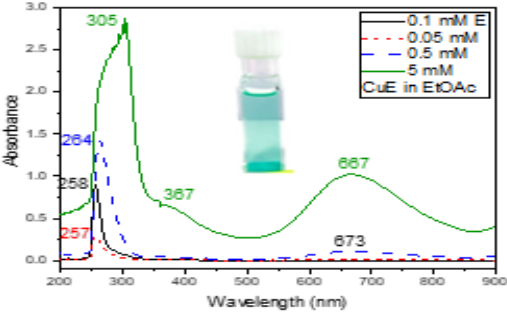
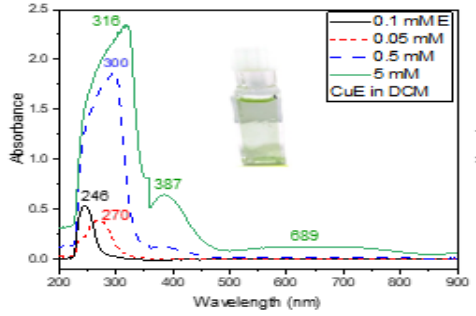


Figure 17: Absorption spectrum of 0.1 mM (black) of ethyl acetoacetate, 0.05 mM (red), 0.5 mM (blue) and 5 mM (green) of CuE complex in EtOAc. at r.t using quartz cell with path length of 1 cm.



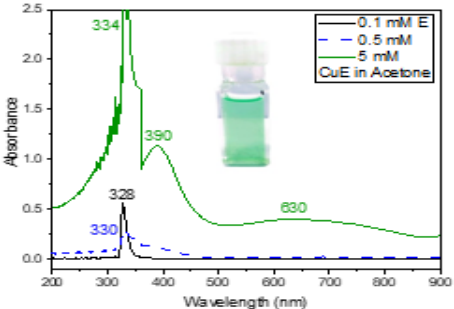
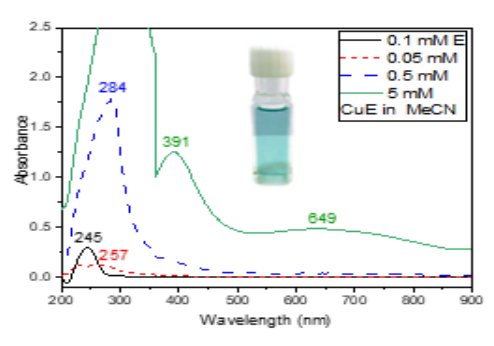


Figure 18: Absorption spectrum of 0.1 mM (black) of ethyl acetoacetate, 0.05 mM (red), 0.5 mM (blue) and 5 mM (green) of CuE complex in DCM.

Figure 19: Absorption spectrum of 0.1 mM (black) of ethyl acetoacetate, 0.5 mM (blue) and 5 mM (green) of CuE complex in Acetone.



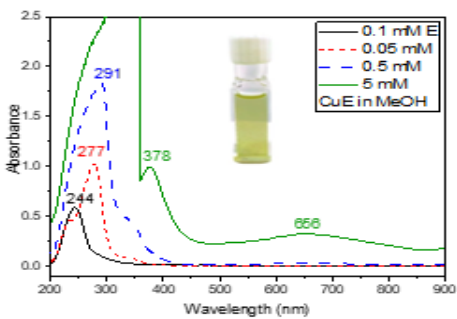
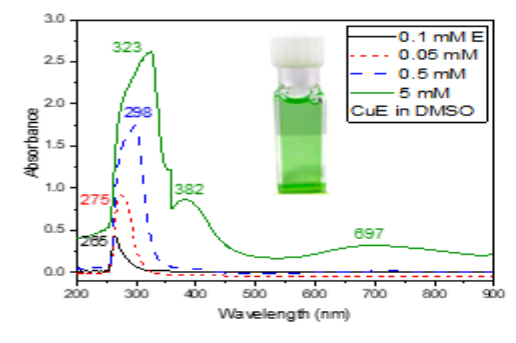


Figure 20: Absorption spectrum of 0.1 mM (black) of ethyl acetoacetate, 0.05 mM (red), 0.5 mM (blue) and 5 mM (green) of CuE complex in MeCN.

Figure 21: Absorption spectrum of 0.1 mM (black) of ethyl acetoacetate, 0.05 mM (red), 0.5 mM (blue) and 5 mM (green) of CuE complex in MeOH.



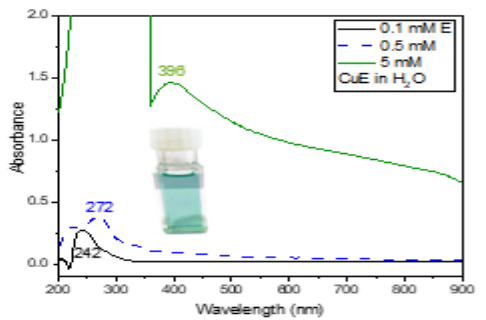
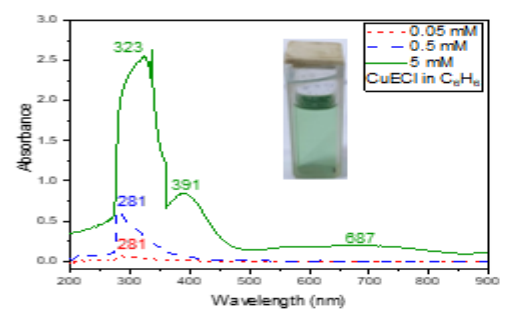


Figure 22: Absorption spectrum of 0.1 mM (black) of ethyl acetoacetate, 0.05 mM (red), 0.5 mM (blue) and 5 mM (green) of CuE complex in DMSO.

Figure 23: Absorption spectrum of 0.1 mM (black) of ethyl acetoacetate, 0.5 mM (blue) and 5 mM (green) of CuE complex in H_2O .



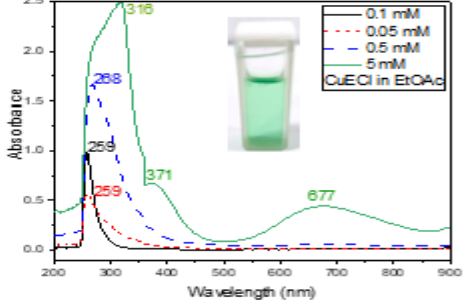
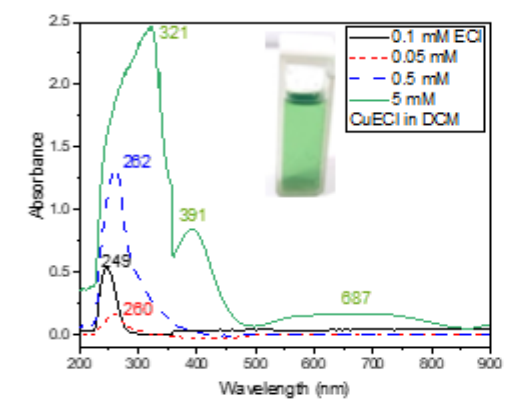


Figure 24: Absorption spectrum of 0.05 mM (red), 0.5 mM (blue) and 5 mM (green) of CuECl complex in C_6H_6 .

Figure 25: Absorption spectrum of 0.1 mM (black) of ethyl4-chloro acetoacetat, 0.05 mM (red), 0.5 mM (blue) and 5 mM (green) of CuECl complex in EtOAc.



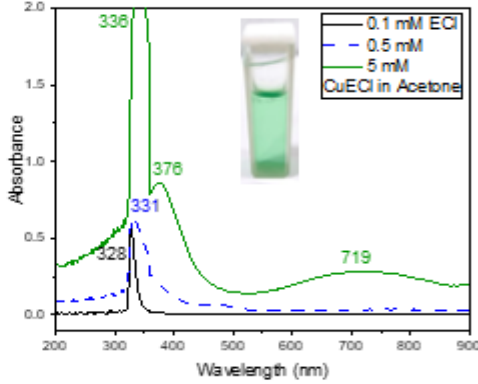
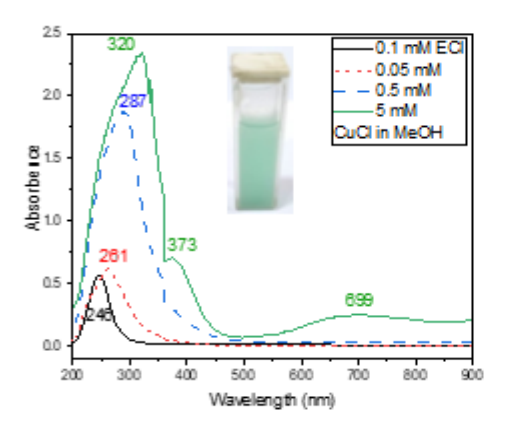


Figure 26: Absorption spectrum of 0.1 mM (black) of ethyl4-chloro acetoacetat, 0.05 mM (red), 0.5 mM (blue) and 5 mM (green) of CuECl complex in DCM.

Figure 27: Absorption spectrum of 0.1 mM (black) of ethyl4-chloro acetoacetat, 0.5 mM (blue) and 5 mM (green) of CuECl complex in Acetone.



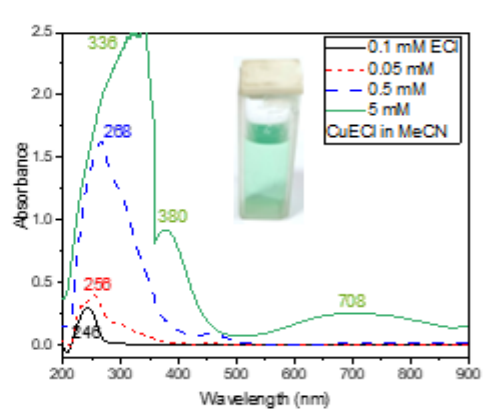
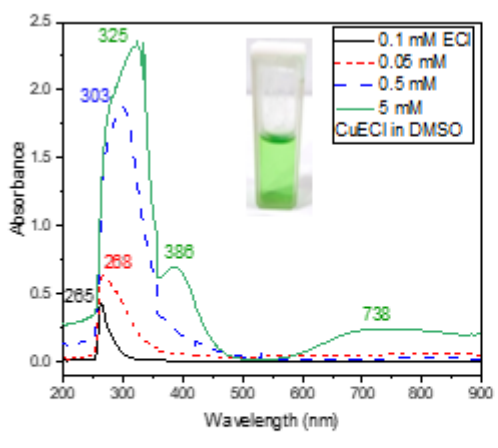


Figure 28: Absorption spectrum of 0.1 mM (black) of ethyl4-chloro acetoacetat, 0.05 mM (red), 0.5 mM (blue) and 5 mM (green) of CuECl complex in MeOH.

Figure 29: Absorption spectrum of 0.1 mM (black) of ethyl4-chloro acetoacetat, 0.05 mM (red), 0.5 mM (blue) and 5 mM (green) of CuECl complex in MeCN.



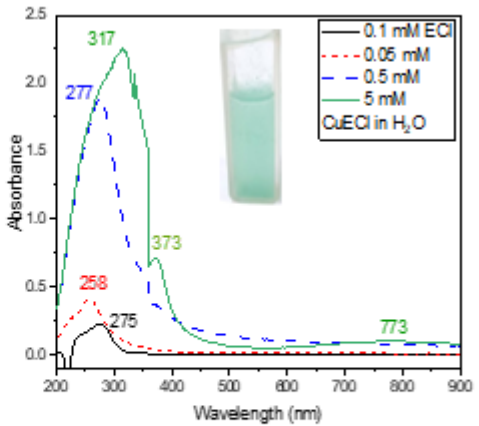


Figure 30: Absorption spectrum of 0.1 mM (black) of ethyl4-chloro acetoacetat, 0.05 mM (red), 0.5 mM (blue) and 5 mM (green) of CuECl complex in DMSO.

Figure 31: Absorption spectrum of 0.1 mM (black) of ethyl4-chloro acetoacetat, 0.05 mM (red), 0.5 mM (blue) and 5 mM (green) of CuECl complex in H₂O.

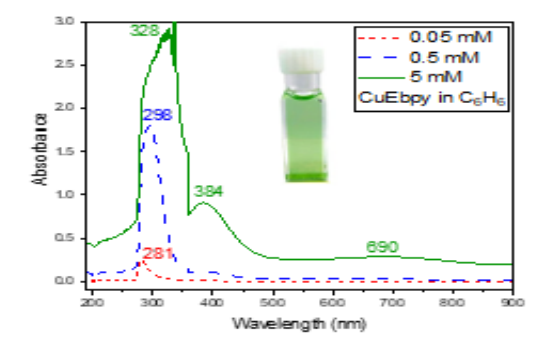
Table 5: Absorption data of E, CuE and Cu(OAc)2 in different solvents.

Complex	Solvent	Concentration (mM)	$\lambda_{max}/nm \ (\epsilon/M^{-1}. cm^{-1})$
CuE	MeOH	0.05	277 (20540)
		0.5	291 (3648)
		5	656 (70), 378 (199)
E		0.1	244 (5880)
CuE	MeCN	0.05	257 (2520)
		0.5	284 (3562)
		5	649 (113), 391 (251)
E		0.1	245 (2970)
CuE	DMF	0.05	274 (5600)
		0.5	299 (3658)
		5	688 (71), 386 (195), 326 (564)
E		0.1	270 (3830)
Cu(OAc)2		1	696 (268), 362 (198), 280 (1667)
		5	704 (181), 296 (417)
CuE	DMSO	0.05	275 (18340)
		0.5	298 (3498)
		5	697 (64), 382 (174), 323 (524)
E		0.1	265 (4300)
CuE	Water	0.5	272 (758)
		5	396 (292)
E		0.1	242 (2720)

Complex	Solvent	Concentration (mM)	$\lambda_{\text{max}}/\text{nm} \ (\epsilon/\text{M}^{-1}.\ \text{cm}^{-1})$
CuE	Benzene	0.05	282 (4200)
		0.5	296 (3618)
		5	650 (47), 392 (188), 324 (536)
CuE	EtOAc	0.05	257 (5760)
		0.5	673 (216), 264 (2846)
		5	667 (204), 367 (130), 305 (575)
E		0.1	258 (8940)
CuE	DCM	0.05	270 (7860)
		0.5	300 (3748)
		5	689 (26), 387 (129), 316 (470)
E		0.1	246 (5370)
CuE	Acetone	0.5	330 (604)
		5	630 (80), 390 (227), 334 (850)
E		0.1	328 (8010)
CuE	EtOH	0.05	278 (10340)
		0.5	291 (13684)
		5	379 (213), 653 (67)
E]	0.1	246 (5250)
Cu(OAc)2]	1	706 (136), 273 (1722)
		5	700 (123), 300 (424)

Table 6: Absorption data of ECl, CuECl and Cu(OAc)2 in different solvents.

Complex Solvent Concentration (mM) λ _{max} /nm (ε/M ⁻¹ , cm	
ECI 0.1 246 (5710) CuECI MeCN 0.05 256 (7960) 0.5 268 (3252) 5 708 (52), 380 (185), 336 (20 ECI 0.1 246 (5510) CuECI DMF 0.05 273 (8460) 0.5 292 (3642)	
ECI 0.1 246 (5710) CuECI MeCN 0.05 256 (7960) 0.5 268 (3252) 5 708 (52), 380 (185), 336 (20 0.1 0.2 0.1 0.2 0.1 0.1 0.1 0.1 0.1 0.1 0.1 0.1 0.1 0.1	
CuECI MeCN 0.05 256 (7960) 0.5 268 (3252) 5 708 (52), 380 (185), 336 (20 ECI 0.1 246 (5510) CuECI DMF 0.05 273 (8460) 0.5 292 (3642)	471)
CuECI MeCN 0.05 256 (7960) 0.5 268 (3252) 5 708 (52), 380 (185), 336 (20 ECI 0.1 246 (5510) 246 (5510) CuECI DMF 0.05 273 (8460) 0.5 292 (3642) 292 (3642)	
0.5 268 (3252) 5 708 (52), 380 (185), 336 (20 EC1 0.1 246 (5510) CuEC1 DMF 0.05 273 (8460) 0.5 292 (3642)	
5 708 (52), 380 (185), 336 (20 ECI 0.1 246 (5510) CuECI DMF 0.05 273 (8460) 0.5 292 (3642)	
ECI 0.1 246 (5510) CuECI DMF 0.05 273 (8460) 0.5 292 (3642)	000)
0.5 292 (3642)	,
0.5 292 (3642)	
5 727 (47) 296 (156) 226 (1021
ECI 737 (47), 386 (156), 326 (4	102)
Cu(OAc) ₂ 1 696 (268), 362 (198), 280	(1667)
5 704 (181), 296 (417)	(100/)
CuECI DMSO 0.05 268 (12660)	
0.5 303 (3748)	
5 738 (50), 386 (141), 325 (470)
ECI 0.1 265 (4300)	
CuECl Water 0.05 258 (8320)	
0.5 277 (3768)	
5 773 (25), 373 (142), 317 (45	50)
ECI 0.1 275 (2330)	
CuECl Benzene 0.05 281 (1300)	
0.5 281 (1292)	
5 687 (39), 391 (170), 323 (51	13)
CuECl EtOAc 0.05 259 (11440)	
0.5 268 (3334)	
5 677 (89), 371 (135), 316 (49	99)
ECI 0.1 259 (8940)	
CuECl DCM 0.05 260 (3500)	
0.5 262 (2676)	
5 687 (35), 391 (170), 321 (49	94)
ECI 0.1 249 (5330)	
CuECl Acetone 0.5 331 (1284)	
5 719 (94), 376 (193), 336 (20	000)
ECI 0.1 328 (8010)	
CuECl EtOH 0.05 257 (8260)	
0.5 292 (3744)	
5 697 (51), 378 (179), 336 (20	000)
ECI 0.1 250 (9460)	
Cu(OAc) ₂ 1 706 (136), 273 (1722)	
5 700 (123), 300 (424)	



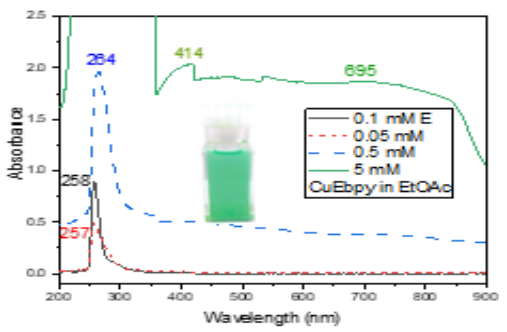
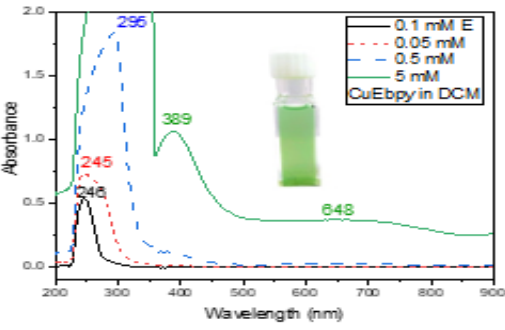


Figure 32: Absorption spectrum of 0.05 mM (red), 0.5 mM (blue dash line) and 5 mM (green) of CuEbpy complex in C_6H_6 .

Figure 33: Absorption spectrum of 0.1 mM (black) of ethyl acetoacetate, 0.05 mM (red), 0.5 mM (blue dash line) and 5 mM (green) of CuEbpy complex in EtOAc.



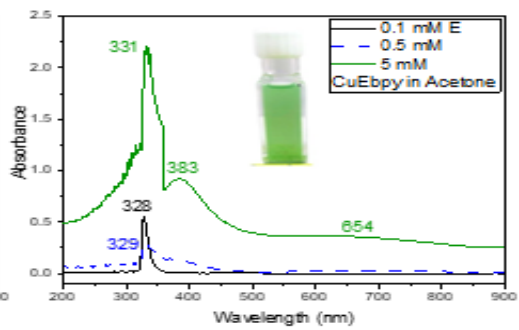
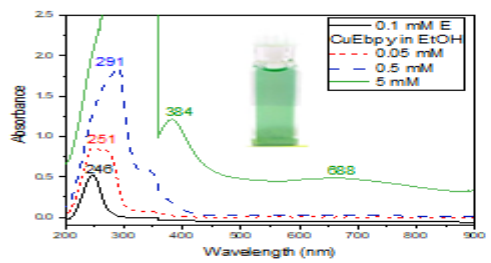


Figure 34: Absorption spectrum of 0.1 mM (black) of ethyl acetoacetate, 0.05 mM (red short dash line), 0.5 mM (blue) and 5 mM (green) of CuEbpy complex in DCM.

Figure 35: Absorption spectrum of 0.1 mM (black) of ethyl acetoacetate, 0.5 mM (blue) and 5 mM (green) of CuEbpy complex in Acetone.



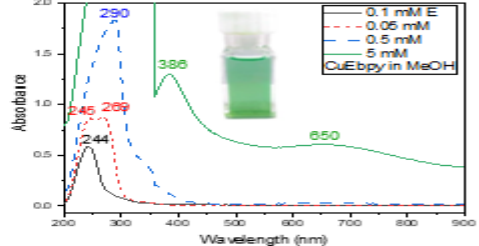
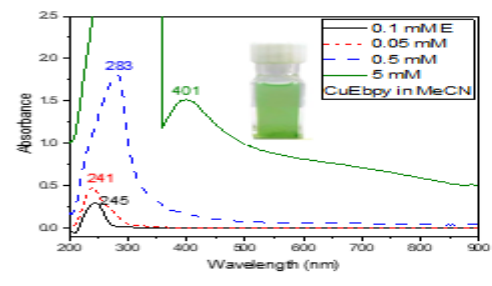


Figure 36: Absorption spectrum of 0.1 mM (black) of ethyl acetoacetate, 0.05 mM (red), 0.5 mM (blue) and 5 mM (green solid line) of CuEbpy complex in EtOH.

Figure 37: Absorption spectrum of 0.1 Mm (black) of ethyl acetoacetate, 0.05 mM (red), 0.5 mM (blue dash line) and 5 mM (green) of CuEbpy complex in MeOH.



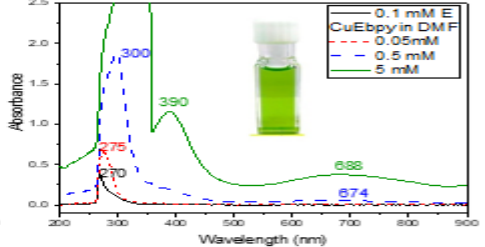
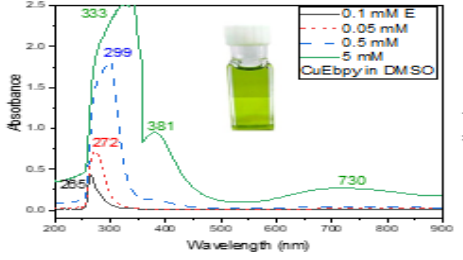


Figure 38: Absorption spectrum of 0.1 mM (black) of ethyl acetoacetate, 0.05 mM (red), 0.5 mM (blue) and 5 mM (green) of CuEbpy complex in MeCN.

Figure 39: Absorption spectrum of 0.1 mM (black) of ethyl acetoacetate, 5 mM (purple) of copper acetate, 0.05 mM (red), 0.5 mM (blue) and 5 mM (green solid line) of CuEbpy complex in DMF.



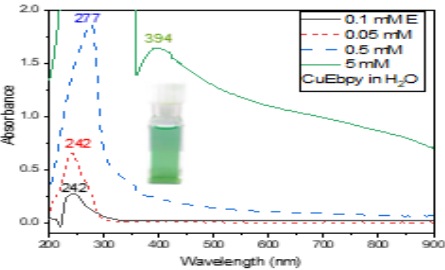
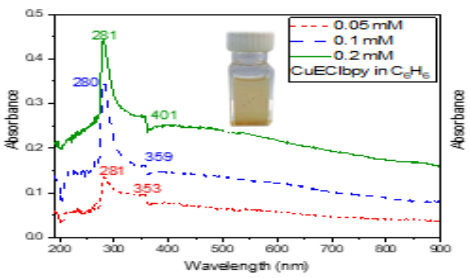


Figure 40: Absorption spectrum of 0.1 mM (black) of ethyl acetoacetate, 0.05 mM (red), 0.5 mM (blue) and 5 mM (green) of CuEbpy complex in DMSO.

Figure 41: Absorption spectrum of 0.1 mM (black) of ethyl acetoacetate, 0.05 mM (red), 0.5 mM (blue dash line) and 5 mM (green) of CuEbpy complex in H₂O.



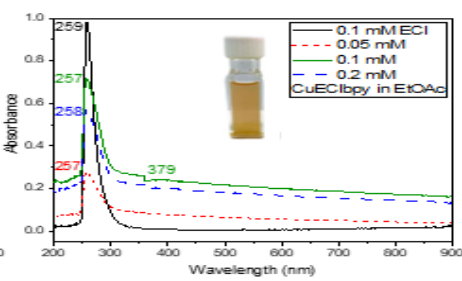
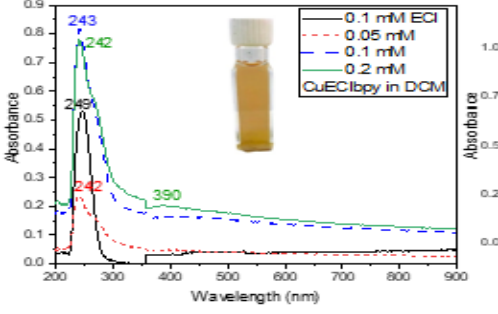


Figure 42: Absorption spectrum of 0.05 mM (red), 0.1 mM (blue) and 0.2 mM (green) of CuEClbpy complex in C_6H_6 .

Figure 43: Absorption spectrum of 0.1 mM (black) of ethyl4-chloro acetoacetat, 0.05 mM (red), 0.1 mM (blue) and 0.2 mM (green) of CuEClbpy complex in EtOAc.



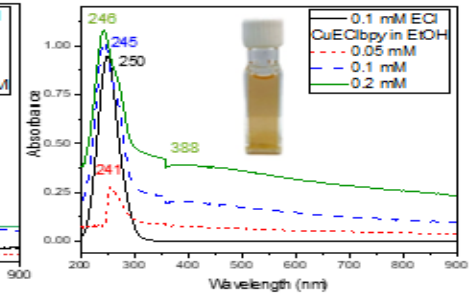
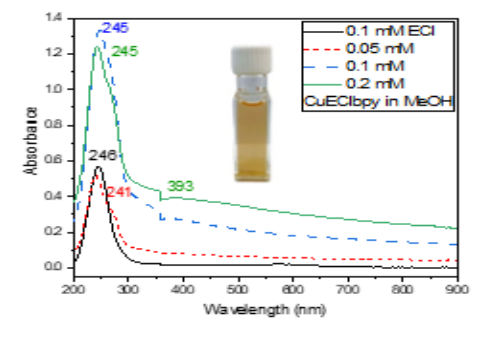


Figure 44: Absorption spectrum of 0.1 mM (black) of ethyl4-chloro acetoacetat, 0.05 mM (red), 0.1 mM (blue) and 0.2 mM (green) of CuEClbpy complex in DCM.

Figure 45: Absorption spectrum of 0.1 mM (black) of ethyl4-chloro acetoacetate, 0.05 mM (red), 0.5 mM (blue) and 5 mM (green) of CuEClbpy complex in EtOH.



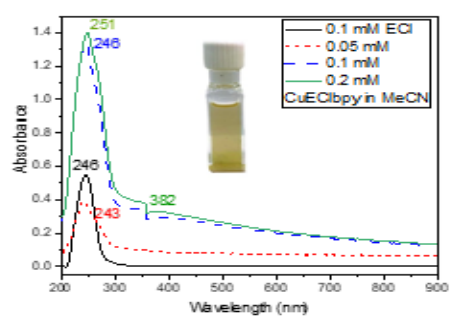


Figure 46: Absorption spectrum of 0.1 mM (black) of ethyl4-chloro acetoacetat, 0.05 mM (red), 0.1 mM (bl ue) and 0.2 mM (green) of CuEClbpy complex in MeOH.

Figure 47: Absorption spectrm of 0.1 mM (black) of ethyl4-chloro acetoacetat, 0.05 mM (red short dash line), 0.1 mM (blue) and 0.2 mM (green) of CuEClbpy complex in MeCN.

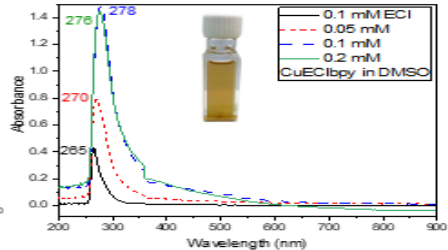


Figure 48: Absorption spectrum of 0.1 mM (black) of ethyl4-chloro acetoacetate, 5 mM (purple) of copper acetate, 0.05 mM (red), 0.1 mM (blue) and 0.2 mM (green) of CuEClbpy complex in DMF.

Figure 49: Absorption spectrum of 0.1 mM (black) of ethyl4-chloro acetoacetat, 0.05 mM (red), 0.1 mM (blue) and 0.2 mM (green) of CuEClbpy complex in DMSO.

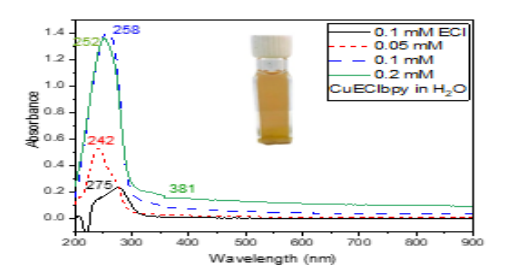


Figure 50: Absorption spectrum of 0.1 mM (black) of ethyl4-chloro acetoacetate, 0.05 mM (red), 0.1 mM (blue) and 0.2 mM (green) of CuEClbpy complex in $\rm H_2O$.

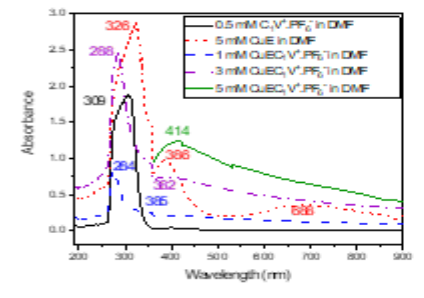
Table 7: Absorption data of E, CuEbpy and Cu(OAc)2 in different solvents.

Complex	Solvent	Concentration (mM)	$\lambda_{\text{max}}/\text{nm} (\epsilon/\text{M}^{-1}.\text{cm}^{-1})$
CuEbpy	Benzene	0.05	281 (5060)
		0.5	298 (3690)
		5	690 (58), 384 (182), 328 (585)
CuEbpy	EtOAc	0.05	257 (9680)
Campy		0.5	264 (3922)
		5	695 (373), 414 (408)
E		1.0	258 (8940)
CuEbpy	DCM	0.05	245 (14700)
		0.5 5	295 (3696)
E	1	0.1	648 (71), 389 (213)
CuEbpy	Acetone	0.5	246 (5370)
Curopy	zeecone		329 (582)
		5	654 (71), 383 (184), 331 (441)
E		0.1	328 (8010)
CuEbpy	EtOH	0.05	251 (174)
		0.5	291 (3722)
		5	688 (97), 384 (242)
E	1	0.1	246 (5250)
Cu(OAc) ₁	1	1	706 (273), 136 (1722)
		5	700 (123), 300 (424)
CuEbpy	MeOH	0.05	269 (176)
		0.5	290 (3670)
		5	650 (126), 386 (260)
E	1	0.1	244 (5880)
CuEbpy	MeCN	0.05	241 (9580)
		0.5	283 (3618)
		5	401 (303)
E	1	1.0	245 (2970)
CuEbpy	DMF	0.05	275 (13120)
		0.5	674 (114), 300 (3776)
		5	688 (76), 390 (231)
E		0.1	270 (3830)
Cu(OAc) ₂		1	696 (268), 362 (198), 280 (1667)
		5	704 (181), 296 (417)
bpy	1	0.25	313 (7748)
CuEbpy	DMSO	0.05	272 (14400)
		0.5	299 (3654)
		5	730 (54), 381 (190), 333 (1999)
E		0.1	265 (4300)
CuEbpy	Water	0.05	242 (13100)
		0.5	277 (3732)
		5	394 (328)
E		0.1	242 (2720)

Table 8: Absorption data of ECl, CuEClbpy and Cu(OAc): in different solvents.

Complex	Solvent	Concentration (mM)	$\lambda_{\text{max}}/\text{nm} \ (e/\text{M}^{-1}, \text{cm}^{-1})$
CuECIbpy	Benzene	0.05	353 (1960), 281 (2720)
		1.0	359 (1640), 280 (3480)
		0.2	401 (1265), 281 (2205)
CuEClbpy	EtOAc	0.05	257 (5560)
синскору	2.00.744	0.1	258 (7180)
		0.2	379 (1020), 257 (2860)
ECI		1.0	259 (8939)
CuECIbpy	DCM	0.05	242 (4740)
		1.0	243 (8170)
		0.2	390 (1020), 242 (3895)
ECI		0.1	249 (5330)
CuECIbpy	EtOH	0.05	241 (6940)
		0.1	245 (10260)
		0.2	388 (1965), 246 (5405)
ECI	Benzene	0.1	250 (9460)
Cu(OAc) ₂		1	706 (273), 136 (1722)
		5	700 (123), 300 (424)
CuECIbpy		0.05	
		1.0	353 (1960), 281 (2720)
		0.2	359 (1640), 280 (3480)
			401 (1265), 281 (2205)
CuECIbpy	EtOAc	0.05	257 (5560)
		0.1	258 (7180)
		0.2	379 (1020), 257 (2860)
ECI		0.1	259 (8939)
CuECIbpy	MeOH	0.05	241 (10320)
		0.1	245 (6215)
		0.2	393 (1970), 245 (6215)
ECI		0.1	246 (5710)
CuECIbpy	MeCN	0.05	1 1
			243 (7880)
		0.1	246 (13480)
		0.2	382 (1725), 251 (7020)
ECI		0.1	246 (5510)
CuEClbpy	DMF	0.05	272 (11840)
		0.1	276 (6640)
		0.2	379 (1470), 276 (6640)
ECI		0.1	271 (7080)
Cu(OAc) ₂		1	696 (268), 362 (198), 280 (1667)
		5	704 (181), 296 (417)
bpy		0.25	313 (7748)

Complex	Solvent	Concentration (mM)	$\lambda_{\text{max}}/\text{nm} (e/\text{M}^{-1}.\text{cm}^{-1})$
CuECIbpy	DMSO	0.05	270 (15820)
		0.1	278 (14850)
		0.2	276 (7220)
ECI		0.1	265 (4300)
CuECIbpy	Water	0.05	242 (10580)
		0.1	258 (13970)
		0.2	381 (860), 252 (6820)
ECI		0.1	275 (2330)



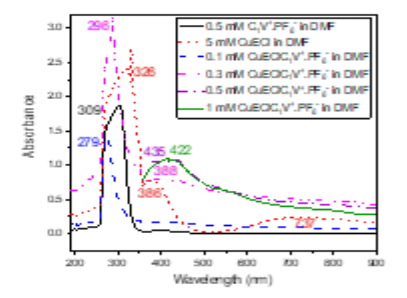


Figure 51: Absorption spectra of 0.5 mM (black) of C₁V⁺.PF₆, 5 mM (red) of CuE, 1 mM (blue), 3 mM (purples) and 5 mM (green) of CuEC₁V⁺.PF₆ complex in DMF.

Figure 52: Absorption spectra of 0.5 mM (black) of $C_1V^+PF_{e'}$, 5 mM (red) of CuECl, 0.1 mM (blue), 0.3 mM (magnet) and 0.5 mM (purple) of $CuEClC_1V^+PF_{e'}$ complex in DMF.

Table 9: Absorption data of CuEC₁V⁺. PF₆⁻ and CuEClC₁V⁺. PF₆⁻ in DMF solvent.

Complex	Solvent	Concentration (mM)	$\lambda_{ m max}/{ m nm}~(arepsilon/{ m M}^{-1}.~{ m cm}^{-1})$
CuEC ₁ V ⁺ . PF ₆ ⁻	DMF	1	382 (217), 274 (841)
		3	382 (249), 288 (819)
		5	414 (248)
CuEClC ₁ V ⁺ . PF ₆ ⁻	DMF	0.1	279 (1432)
		0.3	388 (2623), 296 (9526)
		0.5	435 (2168)
		1	422 (1094)

The recorded spectra reveal bands originating from internal d-orbital transitions to CuE, CuECl and $\text{Cu}(\text{OAc})_2$ occurred in ethanol at 653 nm, 697 nm and 700 nm correspondingly, and occurred in DMF at 688 nm, 737 nm and 704 nm respectively. The d-orbital transitions of CuE and CuECl are shifted to shorter λ by 47 nm and 3 nm corresponding in ethanol and by 16 and 33 nm respectively in DMF compare to those of $\text{Cu}(\text{OAc})_2$ [33]. These two blue shifts reflect that the complexation happened among Cu^{2+} metal ion and each of E and ECl. Also, these shifts support that the ligand E is stronger that the ligand ECl. The UV absorption bands occurred at 278 nm and 257 nm for CuE and CuECl respectively in ethanol are blue shifted compared to that of copper acetate (at 300 nm) which reflect harder uv absorption transitions in the complexes. The ligand E absorbs at 246 nm, 328 nm, 258 nm, 245 nm, 246 nm, 244 nm, 270 nm, 265 and 242 nm Acetone in DCM, EtOAC, MeCN, EtOH, MeOH, DMF, DMSO and H₂O acetone. The ligand ECl absorbs at 249 nm, 328 nm, 259 nm, 246 nm, 250 nm, 246 nm, 271 nm 265 nm and 275 nm in same solvents correspondingly [34]. These uv absorptions of both E and ECl are oscillatory with increasing of the dielectric strength of the solvent medium [35].

E and ECl, there is hydrogen bonding within their structures in solutions, the hydrogen bonding supports the resonance and decrease more the energy of π - π * transition. Also, Hydrogen bonding interactions tend to reduce the intensity of the $n-\pi^*$ transition, causing it to undergo a noticeable blue shift. As a result, this transition moves closer in energy to the $\pi-\pi^*$ transition. Consequently, the strong π – π * absorption band overlaps with the weaker n– π * band in both ligands E and ECl [35]. Moreover, the absorption maxima of ligand ECl (249, 328, 259, 246, 250, 246, 271, 265, and 275 nm) appear at slightly longer wavelengths compared with those of ligand E (246, 328, 258, 245, 246, 244, 270, 265, and 242 nm), indicating a red shift for the weaker ligand [35]. This reflects the energetically easier transitions for the ligand ECl compared with the ligand E in the uv region of the spectrum. These easier uv transition could be related to the longer extended conjugation system in the ligand ECl due to the existence of Cl atom compared with that of the ligand E. Except for ECl in H₂O, Both the complexes: CuE and CuECl showed red shifted uv transitions compared with those of the ligand: E and ECI respectively. The easier uv transition of the complexes could be related that upon complexation with Cu²⁺ ion, the well-known structure of the free ligands E and ECl turns into the more planar geometry of the ligands in the complexes CuE and CuECl respectively [36]. This planarity enhances the electron delocalization or resonance in the complex structure compared with the case of the free ligands which ted to red shifts in the uv absorptions of the complexes. The shifts in spectral position and the changes in absorption strength between ligands and their copper(II) derivatives indicate that coordination has taken place. Such modifications suggest that the resulting metal complexes possess a greater degree of planarity than the uncoordinated ligands [37-38].

Visible spectral bands are produced due to excitations of electrons between the split energy levels within the d-orbitals. In the visible region of the spectrum, both of CuE and CuECl showed two bands (except for CuE in H_2O), sharp band of higher energy and the second is broad with lower energy in different solvents arising from electronic transitions among the d-orbitals of the bound Cu(II) ion [38].

For **CuE**, the higher intensity visible bands occurred at 392 nm (benzene), 387 nm (DCM), 390 ma (acetone), 367 nm (EtOAC), 391 nm (MeCN), 379 nm (EtOH), 378 nm (MeOH), 386 nm (DMF), 382 nm (DMSO) and 396 nm (H₂O). Also, CuECl absorbs at 391 nm, 391 nm, 376 nm, 371 nm, 380 nm, 378 nm, 378 nm, 386 nm, 386 nm and 373 nm in benzene, DCM, acetone, EtOAc, MeCN, EtOH, MeOH, DMF, DMSO and H₂O respectively. This band can be assigned to the electronic transition dxz, dyz \rightarrow dxy ($^{36-37}$). Two weak-defined bands appeared in each of **CuE** and **CuECl** as one broad band due to dx² – y² \rightarrow dxy and dz² \rightarrow dxy transitions respectively. This broad band occurred at 687 nm, 687 nm, 719 nm, 708 nm, 697 nm, 656 nm, 737 nm, 738 nm and 773 nm in benzene, DCM, acetone, EtOAc, MeCN, EtOH, MeOH, DMF, DMSO and H₂O respectively. In same solvents, (except H₂O), **CuE** showed this broad band at 650 nm, 689 nm, 630 nm, 667 nm, 649 nm, 653 nm, 656 nm, 688 nm and 697 nm respectively. These three single electron d-d transitions are consonant with square planar **CuE** and **CuECl** complexes (Cu^{2+} with a d⁹ configuration). The square planer Cu^{2+} d⁹ configuration has four-fold splitting with decreasing energy in the following order: dxz, dyz < dz² < d² x² - y² < dxy ($^{133, 34-46}$).

The reactions (axial wordinations) of **bpy**, $C_1V^+.PF_6^-$ and $V_2^{2+}.PF_6^-$ with each of **CuE** and **CuECl** at lab temperature afforded their adducts as precipitates from DMF media: **CuEbpy** and **CuEClbpy**, **CuEC**₁ $V^+.PF_6^-$ and **CuEClC**₁ $V^+.PF_6^-$,

CuEV₂²⁺.2PF₆ and CuECIV₂²⁺.2PF₆ respectively.

These resulted complexes have notable different physical properties compared with their precursor complexes (CuE and CuECl) like their TLC behavior, solubilities, colors and melting point [41-42].

The uv transitions of **CuEbpy** and **CuEClbpy** (Figures 32 to 50) are either the same or blue shitted compared with those of their precursors: **CuE** and **CuECl** respectively. These blue shifts reflect harder uv transitions to happen **CuEbpy** and **CuElbpy** that could be to less charge delocalization due to the axial coordinations with **bpy**.

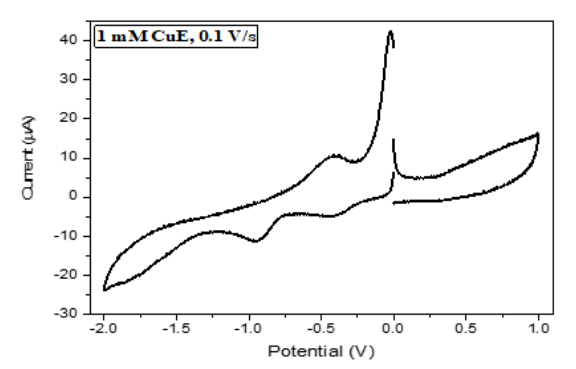
The square planar forms of CuE and CuECl exhibit a characteristic ordering of d-orbital energies: dxz, $dyz < dz^2 < dx^2 - y^2 < dxy$. When these complexes coordinate axially with bpy, structural insights from previously published X-ray data indicate that the copper(II) center in β -diketone complexes preferentially adopts a square pyramidal geometry. In this five-coordinate arrangement, the d-orbital levels shift to the sequence: dxz, $dyz < dx^2 - y^2 < dz^2 < dxy$. This redistribution of energy levels accounts for the observation of three distinct d-d absorption bands in the spectra^[36-37].

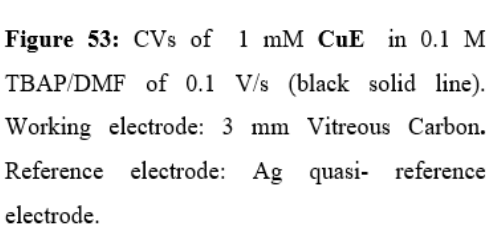
Based on the above interpretations, the transitions of d-electrons of **CuEbpy** be at 384, 690 in benzene, at 389 nm 648 nm in DCM, at 383 nm, 654 nm in acetone, 384 nm, 688 nm in EtOH, 386 nm, 650 nm in MeOH, 390 nm, 688 nm in DMF and 381 nm, 730 nm in DMSO. These d-d transition bands could be assigned to dxz, dyz \rightarrow dxy, and dx² - y² \rightarrow dxy, dz² \rightarrow dxy respectively [39]. The low solubility of **CuEClbpy** prevents the preparation of high concentration solutions (5 mM) in different solvents which led to the disappearance of the low intensity d-d transition band (dx²-y² \rightarrow dxy and dz² \rightarrow dxy). Therefore, only the higher intensity higher energy, d-d transition appeared that is assigned to dxz, dyz \rightarrow dxy transition [39]

The reaction of CuE and CuECl with $C_1V^+.PF_6^-$ at lab temp. for long time results the low yield adducts $CuEC_1V^+.PF_6^-$, $CuEClC_1V^+.PF_6^-$ that have positive axial ligands (very weak ligands). These uncommon complexes are very sparingly soluble complexes showed very exceptional behavior in DMF media. The axial coordinated viologen within these complexes are reduced at dissolving only in DMF at air atmosphere. This reduction is well supported by appearance of the bands at 414 nm, 422 nm in $CuEC_1V^+.PF_6^-$ and $CuEClC_1V^+.PF_6^-$ the resulted viologen radical within the structures of these complexes aren't involved in π -dimerization because of air atmosphere dis-solvation. The reduction happened only at dissolving in DMF media reflects the highly electron deficiency of these axial viologen units within their complexes.

Cyclic Voltammetry

The electrochemical behavior of the ligands (E and ECl), their corresponding copper(II) complexes, and the adducts formed with bpy and ClV+·PF₆⁻ was examined in DMF containing 0.1 M TBAP using cyclic voltammetry (CV). All reported potentials are referenced against a silver pseudo-reference electrode. To prevent chemical oxidation of the electrochemically generated species by air, all measurements were performed at ambient temperature under an argon atmosphere in a conventional three-electrode setup. A glassy carbon disc served as the working electrode, while a platinum wire was used as the counter electrode. Additional experimental parameters for each measurement are detailed in the experimental section or provided in the figure captions. Figures 52 - 63 depict the CVs and the potential data are summarized in Table 10





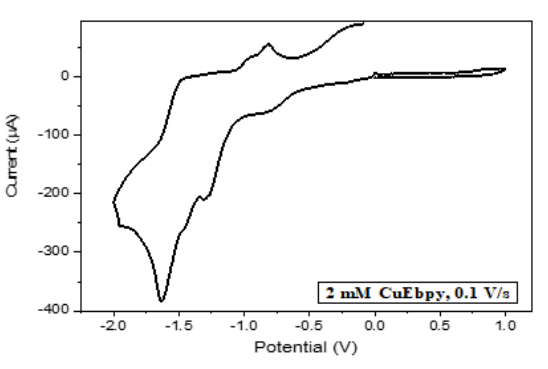
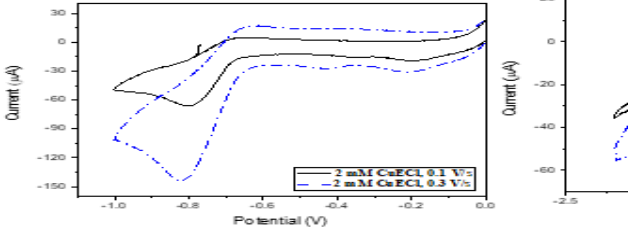


Figure 54: CVs of 2 mM CuEbpy in 0.1 M TBAP/DMF of 0.1 V/s (black solid line). Working electrode: 3 mm Vitreous Carbon. Reference electrode: Ag quasi- reference electrode.



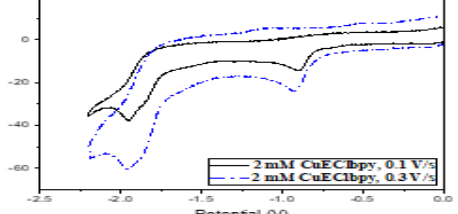
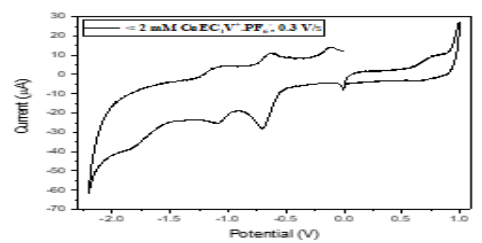


Figure 55: CVs of 2 mM CuECl in 0.1 M TBAP/DMF of 0.1 V/s (black solid line) and 0.3 V/s (blue dash dot line). Working electrode: 3 mm Vitreous Carbon. Reference electrode: Ag quasi-reference electrode.

Figure 56: CVs of 2 mM CuEClbpy in 0.1 M TBAP/DMF of 0.1 V/s (black solid line) and 0.3 V/s (blue dash dot line). Working electrode: 3 mm Vitreous Carbon. Reference electrode: Ag quasireference electrode.



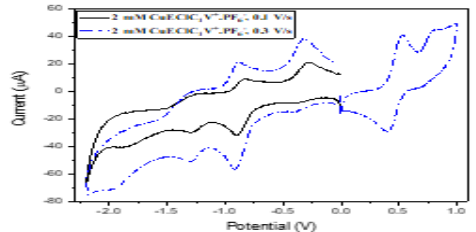
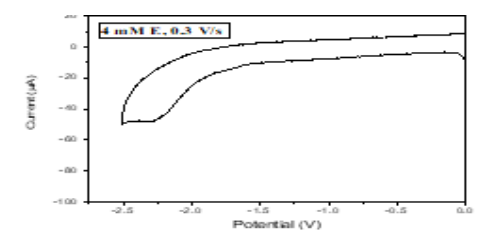


Figure 57: CVs of less than 2 mM CuEC:VT.PF4 in 0.1M TBAP/DMF of 0.3 V/s (black solid line). Working electrode: 3 mm Vitreous Carbon. Reference electrode: Ag quasi-reference electrode.

Figure 58: CVs of 2 mM CuEClC₁V*.PF€ in 0.1M TBAP/DMF of 0.1 V/s (black solid line) and 0.3 V/s (blue dash dot line). Working electrode: 3 mm Vitreous Carbon. Reference electrode: Ag quasi-reference electrode.



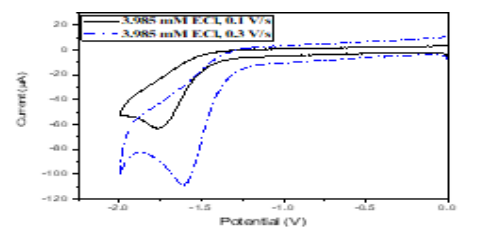
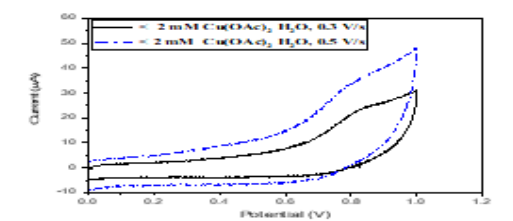


Figure 59: CVs of 4 mM E in 0.1M TBAP/DMF of 0.3 V/s (black solid line). Working electrode: 3 mm Vitreous Carbon. Reference electrode: Ag quasi-reference electrode.

Figure 60: CVs of 3.985 mM ECl in 0.1M TBAP/DMF of 0.1 V/s (black solid line) and 0.3 V/s (blue dash dot line). Working electrode: 3 mm Vitreous Carbon. Reference electrode: Ag quasi-reference electrode.



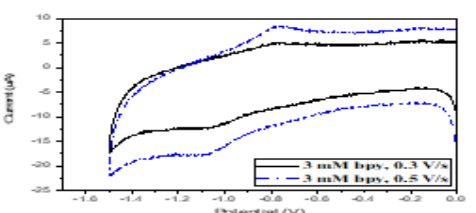


Figure 61: CVs of less than 2 mM Cu(OAC): in 0.1M TBAP/DMF of 0.3 V/s (black solid line) and 0.5 V/s (blue dash dot line). Working electrode: 3 mm Vitreous Carbon. Reference electrode: Ag quasi-reference electrode.

Figure 62: CVs of 3 mM bpy in 0.1M TBAP/DMF of 0.3 V/s (black solid line) and 0.5 V/s (blue dash dot line). Working electrode: 3 mm Vitreous Carbon. Reference electrode: Ag quasi-reference electrode.

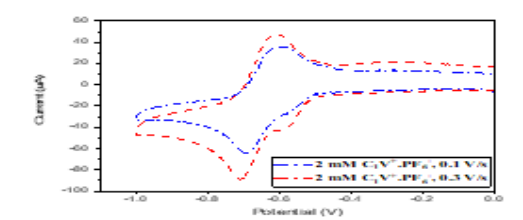


Figure 63: CVs of 2 mM C_1V^* .PF ϵ^* in 0.1M TBAP/DMF of 0.1 V/s (blue dash dot line) and 0.3 V/s (red dash line). Working electrode: 3 mm Vitreous Carbon. Reference electrode: Ag quasi-reference electrode.

Table 10: Experimental voltammetric potentials with number of transferred electrons for The compounds E, ECl and their Cu(II) Complexes Adduct at 0.1 mV/s. A 3 mm glassy carbon electrode was employed as the working electrode, with 0.1 M TBAP in DMF serving as the reference electrode.

Compound	(V/s)	[M]	Epc	Ipc	Epa	Ipa	ΔΕ	E1/2	i_{pa}
			(mV)	(µA)	(mV)	(μA)	(mM)	(mM)	ipe
CuE	0.1		-457.99	-3.71	-22.85	42.5	435.14	-240.42	11.46
CUE		1mM	-957.8	-6.45	-410.76	6.76	547.04	-684.28	1.048
	0.1	2mM	-	-	988.02	15.08	-	-	-
			-198.515	-9.54	-	-	-	-	-
	0.1	2mM	-346.348	-2.49	-	-	-	-	-
CuECl			-804.26	-41.85	-664.632	19.85	139.628	-734.446	0.474 4
Cueci			-207.026	-11.03	-	-	-	-	-
	0.3	2mM	-422.104	-3.91	-	-	-	-	-
			-816.989	-97.84	-646.536	37.75	170.453	-731.763	0.385 8
	0.1	2mM	-1113	25.397	-1093	24.816	20	-1103	0.977 1
			-1680	-12.99	-	-	-	-	-
CuEbpy			-2095	-118.90	-1830	135.45 9	285	-1963	1.139 3
			-	-	457.15	1.515	-	-	-
	0.1	2mM	-	-	899.26	6.92	-	-	-
	0.1	2mM	-910.611	-10.38	-	-	-	-	-
			-1948	-18.17	-	-	-	-	-
	0.3	2mM	-934.687	-18.882	-1041	3.154	- 106.313	-987.844	0.167 04
			-1968	-27.65	-493.57	1.88	1474.43	-1230.79	0.067 99
CuEClbpy			-1871	-39.403	-	-	-	-	-
	0.3	2mM	-646.54	-18.401	-	-	-	-	-
			-	-	-77.9	37.813	-	-	-
			-1326	-35.904	-	-	-	-	-
			-1878	-58.82	-	-	-	-	-
	0.3	2mM	323.651	-6.424	382.99	6.736	59.348	353.325	1.048 5
								1	

Compound	(V/s)	[M]	Epc	Ipc	Epa	Ipa	ΔΕ	E1/2	i _{pa}
			-	_	-	-	(mM)		ipe
			(mV)	(μА)	(mV)	(µA)		(mM)	
		< 2 mM	-413.36	-6.50	-280.18	23.91	133.1 8	-346.77	3.6785
	0.3		-927.86	-41.74	-854.33	19.34	73.53	-891.095	0.4633
CuEC ₁ V ⁺ .PF ₆			-1315	-10.45	-1253	23.18	62	1284	2.2182
	0.3	< 2 mM	-	-	800.043	7.103	-	-	-
		2 mM	- 400.405	-4.031	-277.95	14.90 6	122.5 05	- 339.1525	3.6978
	0.1		- 910.457	-22.957	- 820.976	10.64 3	89.48 1	-865.717	0.4636
	0.1		-1293	-7.397	-1274	12.58	19	-1.2835	1.7017 7
			-1880	-13.006	-	-	-	-	-
			- 413.363	-6.995	- 280.176	23.48 7	133.1 87	-34.6795	3.3576
CuECIC ₁ V ⁺ .			-	-41.816	-854.33	19.22	73.53	-	0.4597
PF6	0.3	2 mM	927.863			5	3	891.0965	
			-1315	-10.418	-1221	- 22.84 2	94	-1.268	2.1925
			-1999	-23.243	-	-	-	-	-
	0.3	2 mM	394.731	-29.308	530.908	37.63 7	136.1 77	462.8195	1.2841
			-	-	808.86	16.35 8	-	-	-
_	0.3	3mM	-1092	-4.423	- 766.229	1.168	325.7 71	929.1145	0.2640
bpy	0.5	3mM	-1113	-6.686	- 766.535	4.412	346.4 65	939.7675	0.6598
	0.3	< 2 mM	-	-	845.67	19.87	-	-	-
Cu(OAc)2	0.5	< 2 mM	-	-	938.29	24.95	-	-	-
E	0.3	4mM	-2027	-27.105	-	-	-	-	-
Eco	0.1	3.985 mM	-1767	-37.47	-	-	-	-	-
ECI	0.3	3.985 mM	-2025	-57.98	-	-	-	-	-
C ₁ V ⁺ .PF ₆		2m	- 930.393	-26.77	-	-	-	-	-
	0.3	М	-1038	-34.65	-902.56	36.06 8	135.4 4	-970.28	0.9606

The cyclic voltammograms (CVs) of the complexes CuE and CuECl are depicted in Figures 49 and 56 respectively. These CVs will be compared with the CVs of their precursor: $Cu(OAc)_2$, E and ECl that are presented in Figures 3.185 – 3.187 respectively. The irreversible reduction of the free ligands E and ECl occurred at -2.1027 V and -2.025 V respectively at f 0.3 V/s. The irreversible oxidation of Cu^{2+} ion in $Cu(OAc)_2$ is noted at 845.666 mv rt 0.3 V/s see Figure 55 and table 11.

The reduction of Cu^{2+} ion in the complexes CuE and CuECl happened at -457.99 mv and -346.348 mv respectively. The easier Cu^{2+} reduction process (-346.348) in the complex CuE compared with that of CuECl (- 4571.19 mv) is consistent with the more electron deficiency of Cu^{2+} ion in the complex CuECl. The reductions of the coordinated E and ECl in the complexes CuE and CuECl respectively are noted at -957.8 mv and -804.26 mv. Here, the coordinated ECl suffers more electron deficiency than the coordinated ECl are anodically shifted compared with the reductions of the free E and ECl. These shifts reflect the decrease of the electron densities of the ligands after complexations. The coordination of ECl by with the complexes ECl and ECl results the adduct complexes ECl and ECl respectively. The ECl and ECl are presented in Figure 3.183, 3.185 and 3.188. The nearly quasi-reversible redox couple was at $E_{1/2} = -939.7675$ mV at 0.5 V/s which is related with one-electron reduction.

The square pyramidal complexes: **CuEbpy** and **CuEClbpy** showed the reduction peaks at -1113 mv, -2095 vm and -910.611 mv, -1948 mv at 0.1 V/s respectively. These two reduction peaks are attributed to reductions of coordinated **bpy**, **E** in **CuEClbpy** and coordinated **bpy**, **E** Cl in **CuEClbpy** respectively. The reductions of coordinated **bpy** in **CuEbpy** and

CuEClbpy are cathodically and anodically shifted compared with that of the free **bpy**. The reduction of coordinated **ECI** in **CuEClbpy** is shift at -181 mv compare to the free **ECI** (occurred at -1767.7 mv for **ECI**). The easier reduction of the coordinated **bpy** in **CuEClbpy** compared to that of the free **bpy** indicates the more electron donating of the coordinated **bpy** into the Cu²⁺ ion compared with the case of the **CuEbpy** (stranger Cu-N bond in **CuEClbpy**). The coordinated **ECI** follows opposite trend that is less coordinated to Cu²⁺ ion compared with coordinated **E** in the **CuEbpy** with led to harder **ECI** reduction with respect to the coordinated **E**.

The reduction of the coordinated copper (II) ion = $Cu^{2+} + 1e^- \rightarrow Cu^+$ is very weak to be determined. At 0.3 V/s, the opposite process: the oxidation of the coordinated Cu^+ in **CuEClbpy** happened at around -493.567 mv. In the positive potential scan, the oxidation of the coordinated Cu(II) in the **CuEbpy** occurred irreversibly at 899.262 mv.

Perfectly, this oxidation of the coordinated Cu(II) in **CuEbpy** is easily happened at (899.262 mv) compared with that of **Cu(OAc)**₂ (at 938.29 mv). This shift reflects the higher electron density of the coordinated Cu(II) compared with that of the free ion.

The CVs of C_1V^+ .**PF**₆ at two voltage scan rates (0.3 V/s and 0.5 V/s) are shown in Figure 3.189. Two redox waves are noted the first is irreversible happened at -930.393 mv and the second is quasi-reversible occurred at -970.28 mv (at 0.3 V/s: $\Delta E=135.44$ mv, $\frac{i_{pa}}{i_{pc}}=0.9606$). They are related to one-electron reduction of C_1V^+ .**PF**₆ to C_1V^+ viologen radical. Upon coordination of C_1V^+ .**PF**₆ to the C_1V^+ .**PF**₆ and C_1V^+ .**PF**₆ and C_1V^+ .**PF**₆, these two reductions are shifted to -708.891 mv, -1103 mv and -927.863 mv -1315 mv respectively at 0.3 V/s. The first and second reductions are easier and harder happened respectively in both complexes. These shifts indicate the higher need to the reduction of C_1V^+ .**PF**₆ after the coordination and the favorability of the formation the intermolecular π -diner C_1V^+ VC_1 within two complexes.

The complex $CuEClC_1V^+.PF_6^-$ showed reduction at - 413.363 mv due to the process $Cu^{2+} + 1e^- \rightarrow Cu^+$ which reoxidized at -280.176 mv ($Cu^+ \rightarrow Cu^{2+} + 1e^-$). This reduction was very weak to be determined in the complex $CuEC_1V^+.PF_6^-$ but the reoxidation was noted at -110.797 mv.

The coordinated **E** and **ECl** in the complexes **CuEC₁V⁺.PF₆** and **CuEClC₁V⁺.PF₆** showed easier reductions at -1873 mv and -1999 mv respectively compared with those of **E** (- 2027 mv) and **ECl** (-2025 mv) respectively. The higher negative shift (easier reduction) of the coordinated **E** compared to **ECl** is wonderfully agreed with the higher election donation of **E** to the Cu²⁺ ion. Therefore, the Cu²⁺ oxidation is easily happened in **CuEC₁V⁺.PF₆** (~ 800.043 mv) compared with the **CuEClC₁V⁺.PF₆** (~808.861 mv) (due to the higher electron density received by Cu²⁺ from **E** than **ECl**)of Cu²⁺ to Cu⁺ ion in **CuEV⁺.PF₆** is consistent with the higher electron deficiency of Cu²⁺ ion than that in **CuEClV⁺.PF₆**.

Our electrochemical results, supported the formation of the complexes and showed well the electronic properties of the coordinated Cu(II) ion, ligands and viologen units

4. Reduction of viologen derivative and its complex

The UV-Visible absorption spectra were obtained after reducing the mixtures using solvation in Zn powder, with concentrations of 0.3 mM of CuEV₂²⁺.2PF₆. Additionally, reduction was carried out using activated zinc powder. The absorption spectra were recorded over a range of 190-900 nm and are presented in Figures 64 - 67 with the corresponding electronic absorption data summarized in Table 11.

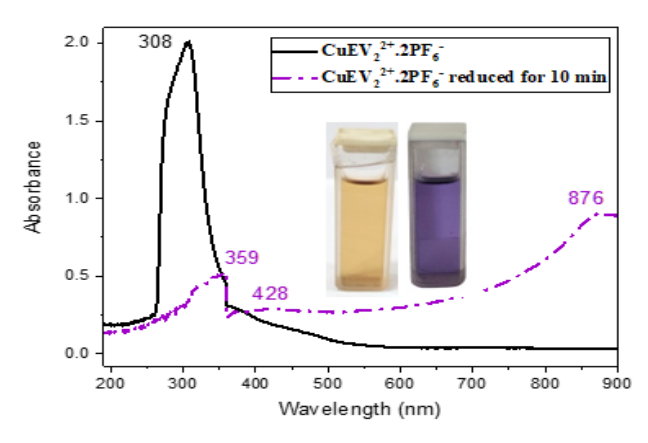


Figure 64: Absorption spectrum of 0.3 mM of **CuEV**₂²⁺**.2PF**₆ (black) and 0.3 mM reduced **CuEV**₂²⁺**.2PF**₆ (purple) by activated zinc powder in DMF. Blank: 0.3 mM **CuEV**₂²⁺**.2PF**₆.

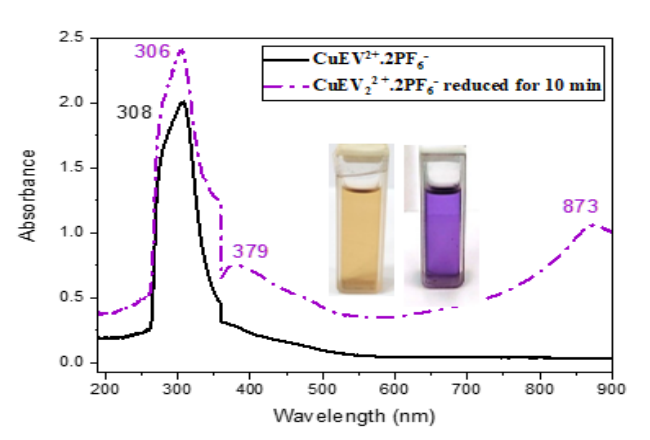
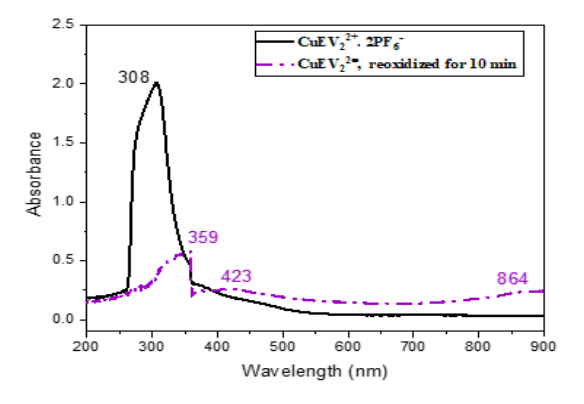


Figure 65: Absorption spectrum of 0.3 mM of $CuEV_2^{2+}.2PF_6^-$ (black) and 0.3 mM reduced $CuEV_2^{2+}.2PF_6^-$ (purple) by activate Zn in DMF. Blank: DMF.



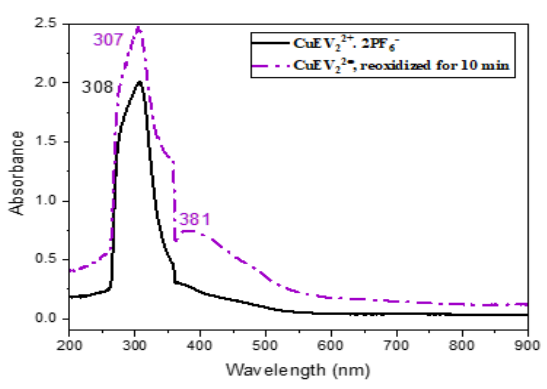


Figure 66: Absorption spectrum of 0.5 mM $\text{CuEV}_2^{2+}.2\text{PF}_6^-$ (black) and 0.3 mM oxidized $\text{CuEV}_2^{2^2}$ (purple) in DMF. Blank: 0.5 mM $\text{CuEV}_2^{2^+}.2\text{PF}_6^-$.

Figure 67: Absorption spectrum of 0.5 mM **CuEV₂²⁺.2PF₆** (black) and 0.3 mM oxidized **CuEV₂²⁻** (purple) in DMF. Blank: DMF.

The adduct Cu (II) complexes (CuEV22+.2PF6-) are reduce with activate Zn and observe by UV-Visible. To monitor all spectral changes after reduction of viologen unites (coordination to Cu (II) ion in adduct complexes and those bonded to the terminal of ligand in complex), two blanks are used in absorption spectra. The first blank is the solvent DMF itself and the second is non-reduced complex solution. The absorption spectra of reduced solution are depicted in Figures 64 – 67 . Table 14 presents the collected data on electronic absorption. In Cu(II)-viologen complexes of CuEV2²⁺.2PF6⁻ reduction leads to the formulation of viologen (V•+), which dimerize into [V•+]2 dimers through strong π - π stacking interactions. The spectral shift from 550–600 nm to 700–800 nm in UV-Vis spectra, As is clearly observed the appearance of peaks at 800 in all compounds , this indicating the occurrence of the process of reduction and the formation of a dimer, confirms dimer formation. The presence of Cu(II) can modulate the stability and redox properties of the dimer, differentiating the behavior of coordinated vs. free viologen radicals [47-50]

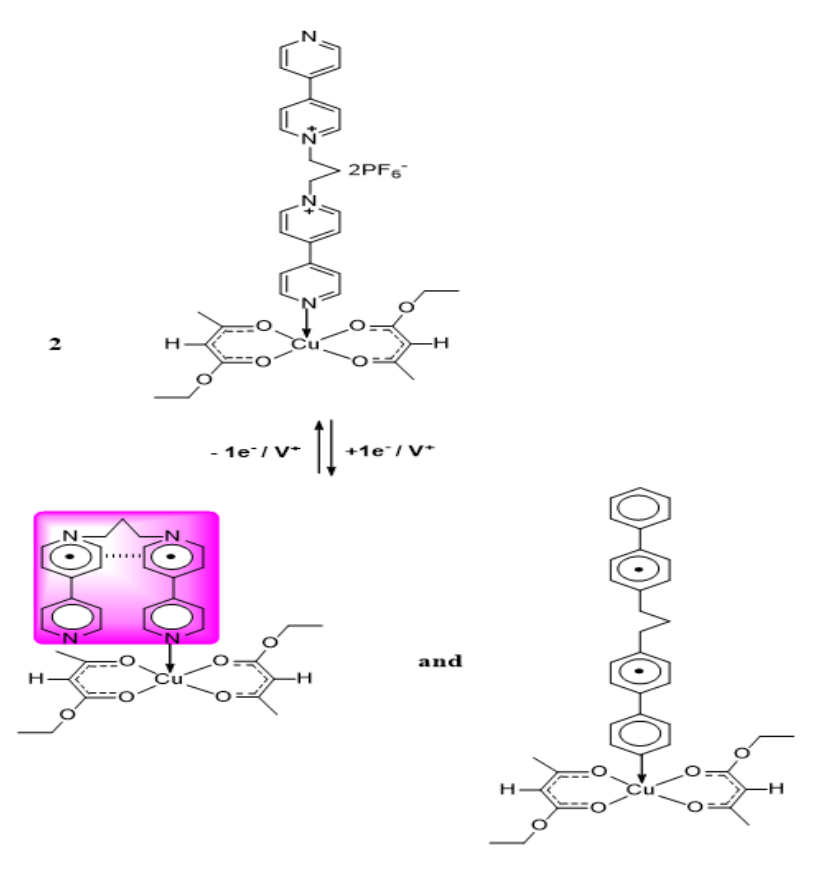


Figure 68: Intra-molecular dimerized viologen radicals of CuEV22+.2PF6 in DMF.

Table 11: The observed electronic-absorption features of CuEV₂²⁺.2PF₆ compounds, their reduced forms by activated zinc powder and reoxidized form by air atmosphere in DMF

Compound	λ max in nm	λ max (nm)							
	(ε in M ⁻¹ .cm)	Blank	:: DMF	Blank: compound soln. in DMF					
		Reduced	Reoxidized	Reduced form	Reoxidized				
		form	form		form				
CuEV ₂ ²⁺ .2PF ₆ ⁻	433 (325)	379 - 873	381	428 - 876	423 - 864				

CONCLUSION

The reaction of two equivalents of ethyl acetoacetate and ethyl 4-chloroacetoacetate with one equivalent of copper(II) acetoacetate resulted in the formation of two primary copper(II) complexes: CuE and CuECl. These complexes were further reacted with 4,4'-bipyridine (bpy) and monoviologen ($C_1V^+.PF_6^-$) to afford the corresponding axial adducts: CuEbpy, CuEClbpy, CuEClV $^+.PF_6^-$, and CuEClClV $^+.PF_6^-$. All synthesized compounds were isolated as solids and characterized using multiple analytical techniques, including FT-IR, mass, XRD, thermal analysis (TGA - DSC), UV-Visible spectroscopy, and cyclic voltammetry. XRD analysis enabled the calculation of crystal sizes (D) using both the williamson—Hall (W–H) method and scherrer equation and the, with strain values derived from the latter. Thermal stability studies showed that CuEClbpy exhibited greater stability than CuEbpy, with the general order of thermal stability being:

 $CuEClC1V^+.PF_6^- > CuEC1V^+.PF_6^- > CuEbpy > CuEC1 > CuEClbpy > CuE$

All decomposition processes were non-spontaneous and endothermic. The formation of adducts was further confirmed via UV-Visible spectroscopy, conducted in various solvents and concentrations (0.05, 0.5 and 5) mM. The d-d transitions of CuE and CuECl in both ethanol and DMF exhibited blue shifts compared to copper(II) acetate, indicating successful complexation and suggesting that ligand E is a stronger donor than ECl. UV absorption bands of CuE and CuECl were also blue-shifted, reflecting the enhanced rigidity and planarity of the complexes, which hinder $\pi \to \pi^*$ and $n \to \pi^*$ transitions. Both ligands E and ECl displayed solvent-dependent UV absorption behavior due to intra- and intermolecular hydrogen bonding, which modulates their transition energies. Upon coordination with Cu²⁺, the complexes exhibited red-shifted UV bands (except in water), attributed to increased planarity and conjugation, enhancing electron delocalization. In the visible region, both CuE and CuECl presented two main d-d transition bands: a high-energy sharp band (dxz, dyz \rightarrow dxy) and a low-energy broad band ($dx^2-y^2/dz^2 \rightarrow dxy$), confirming a square planar geometry consistent with a d⁹ Cu²⁺ configuration. Axial coordination with ligands such as bpy or viologens induced shifts in both UV and d-d transitions, signifying a change in geometry from square planar to square pyramidal. This geometry was supported by literature X-ray structures for similar β-diketone Cu(II) systems. For example, CuEbpy and CuEClbpy exhibited blue-shifted transitions compared to their precursor complexes, attributed to reduced π -delocalization due to axial ligand coordination. In CuEClbpy, only highenergy transitions were observable due to its low solubility and weak absorption in solution. Adducts with viologen ligands (C₁V⁺.PF₆⁻) displayed unusual spectral behavior in DMF, where spontaneous reduction of the axial viologen units occurred in air, producing viologen radicals detected by absorption bands at ~414–422 nm. These radicals did not form π -dimers under atmospheric conditions, reflecting high electron deficiency and unique electronic environments of the coordinated viologen units. Electrochemical studies demonstrated that the coordination of C1V+.PF₆- to Cu(II) in CuEC₁V+.PF₆- and CuEClC₁V⁺.PF₆⁻ significantly altered the redox behavior. The first viologen reduction became easier (shifted to less negative potential), while the second became more difficult, suggesting enhanced electronic interaction and the likely formation of intramolecular π-dimer species (C1V·...VC1). A weak Cu(II)/Cu(I) redox couple was clearly observed in CuEClC₁V⁺.PF₆⁻, and partially in CuEC₁V⁺.PF₆⁻. The ligands E and ECl, upon coordination, showed facilitated reductions compared to their free forms, with ligand E promoting a lower Cu(II) oxidation potential due to its stronger electrondonating ability. Lastly, the interaction of CuE and CuECl with bis-viologen (V₂²⁺.2PF₆⁻) was investigated. The reduction of the resulting complexes (CuEV₂²⁺.2PF₆⁻) was performed using activated zinc in DMF under argon atmosphere. These reductions triggered the redox-responsive behavior of the viologen moieties, forming novel molecular switches, which serve as promising systems for redox-driven molecular devices

REFERENCES

- [1] Monk, P. M. S. "The viologens: physicochemical properties." Synthesis and Applications of the Salts of 4.4 (1999).
- [2] . Michaelis, L., and Edgar S. Hill. "The viologen indicators." The Journal of general physiology 16.6 (1933): 859.
- [3] . Bus, James S., and James E. Gibson. "Paraquat: model for oxidant-initiated toxicity." Environmental health perspectives 55 (1984): 37-46.
- [4] . P. M. S. Monk. The Viologens: Physicochemical Properties, ." Synthesis and Applications of the Salts of 4, 4'-Bipyridine. Chichester: John Wiley & Sons Ltd. 1998.
- [5] . Ben L. Feringo, Molecular Switches, Wiley-VCH Verlag Gmbh 2001.
- [6] . Crespi, Ayelén F., et al. "Montmorillonite materials with paramagnetic metal complexes: Structural studies and catalytic degradation of emerging pollutants." Journal of Environmental Chemical Engineering 11.6

- (2023): 111420.
- [7] Silverstein, R. M., Webster, F. X., & Kiemle, D. J. (2014).
- [8] . Silverstein, R. M., Webster, F. X., & Kiemle, D. J. (2014).
- [9] Dube, N., Porwal, P., & Prasad, R. (1988). Spectroscopic and molecular orbital studies of ethylchloroactate and ethyl bromoacetate. Journal of Raman spectroscopy, 19(3), 189-197.
- [10] . Sebastian, S., Sylvestre, S., Sundaraganesan, N., Karthikeyan, B., & Silvan, S. (2022). Conformational analysis, molecular structure, spectroscopic, NBO, reactivity descriptors, wavefunction and molecular docking investigations of 5, 6-dimethoxy-1-indanone: A potential anti Alzheimer's agent. Heliyon, 8(1).
- [11] . ROBERT J. YORK, WESLEY D. BONDS, JR., BR ILLE P. COTSORADIS, AND RONALD D. ARCHER, β-Diketone Complexes of Cobalt(111). III. Tris(β-dike tona to)cobal t (111) and Bis(acetylacetonato)diaminecobalt(III) Trichelate Species, Inorganic Chemistry, Vol. 8, No. 4,A pril 1969
- [12] . Tayyari, S. F., Zeegers-Huyskens, T., & Wood, J. L. (1979). Spectroscopic study of hydrogen bonding in the enol form of β -diketones Vibrational assignment and strength of the bond. Spectrochimica Acta Part A: Molecular Spectroscopy, 35(11), 1265-1276.
- [13] . Neelakantan, P. "Raman spectrum of ethyl chloroacetate." Proceedings of the Indian Academy of Sciences-Section A. Vol. 59. No. 6. New Delhi: Springer India, 1964.
- [14] . ESHAGHI MALEKSHAH, Rahime, et al. New mononuclear copper (II) complexes from β-diketone and β-keto ester N-donor heterocyclic ligands: structure, bioactivity, and molecular simulation studies. Journal of Coordination Chemistry, 2018, 71.7: 952-968.
- [15] . Holtzclaw, Henry F., et al. "Mass spectra of metal chelates. I. Substituent effects on ionization potentials and fragmentation patterns of some 1-methyl-3-alkyl-1, 3-dione-copper (II) chelates." Journal of the American Chemical Society 91.14 (1969): 3774-3778.
- [16] . Turgambaeva, A. E., A. F. Bykov, and I. K. Igumenov. "Investigation of the thermal decomposition of bis (acetylacetonato) copper (II) vapour by a mass spectrometric method." Thermochimica acta 256.2 (1995): 443-456.
- [17] Azhar H. Gatea, et al. "Ligand Adducts of Bis(acetylacetonato) Copper(II), Bis(3-chloroacetylacetonato) Copper(II) with 4,4'-bipyridine, and Propylene Spacered Bis-viologen." Journal of Medicinal and Chemical Sciences, 6.2 (2023): 280-303.
- [18] . Waseda, Yoshio, Eiichiro Matsubara, and Kozo Shinoda. X-ray diffraction crystallography: introduction, examples and solved problems. Springer Science & Business Media, 2011.
- [19] . Prabhu, Yendrapati Taraka, et al. "X-ray analysis by Williamson-Hall and size-strain plot methods of ZnO nanoparticles with fuel variation." World Journal of Nano Science and Engineering 2014 (2014).
- [20] . Waseda, Yoshio, Eiichiro Matsubara, and Kozo Shinoda. X-ray diffraction crystallography: introduction, examples and solved problems. Springer Science & Business Media, 2011.
- [21] . N. Alrazaq, PHD. Thesis, University of Basrah, 2021.
- [22] . Kim, Yi-Yeoun, et al. "A critical analysis of calcium carbonate mesocrystals." Nature Communications 5.1 (2014): 1-14
- [23] . Rabiei, Marzieh, et al. "Comparing methods for calculating nano crystal size of natural hydroxyapatite using X-ray diffraction." Nanomaterials 10.9 (2020): 1627.
- [24] Zamkovskaya, A., E. Maksimova, and I. Nauhatsky. "Size–strain line-broadening analysis of the calcite-type borates ABO3 (A= Fe, In, Ga)." Journal of Physics: Conference Series. Vol. 1135. No. 1. IOP Publishing, 2018.
- [25] . Lalancette, Roger A., et al. "The thermal decomposition and analyses of metal tris-acetylacetonates: Free radical formation from Al, Cr, Mn, Fe and Co complexes." Journal of Thermal Analysis and Calorimetry 135 (2019): 3463-3470.
- [26] . Alabdali, Ammar J., and Mohammed HA Al-Amery. "Synthesis, Thermal Study and Biological Activity of Cobalt (II) and Copper (II) Mixed Ligand Complexes Using (N-4-Methoxy Phenyl) Amino Phenyl Acetonitrile and Histidine Ligands." Journal of Pharmaceutical Sciences and Research 11.1 (2019): 155-158.
- [27] . Farrukh, Muhammad Akhyar, et al. "Photoluminescence emission behavior on the reduced band gap of Fe doping in CeO2-SiO2 nanocomposite and photophysical properties." Journal of Saudi Chemical Society 23.5 (2019): 561-575.
- [28] SHEIKH, Javed, et al. Synthesis and in vitro biology of Co (II), Ni (II), Cu (II) and Zinc (II) complexes of functionalized beta-diketone bearing energy buried potential antibacterial and antiviral O, O pharmacophore sites. Journal of Saudi Chemical Society, 2013, 17.3: 269-276.
- [29] . Jghebil, H. O., Jassem, I. A., Flafel, I. A., & Abdul, H. W. S. (2023). Axial ligation for copper (II) complexes

- of bis (acetylacetonato) ethylenediimine and bis (3-chloroacetylacetonato) ethylenediimine.
- [30] R. A. Lalancette, D. Syzdek, J. Grebowicz, E. Arslan and I. Bernal, J. Therm. Anal. Calorim., 2018, 13, 8, pp. 1-8.
- [31] .CHRISSAFIS, K.; LALIA-KANTOURI, Maria; ASLANIDIS, Paraskevas. Kinetic analysis of the thermal decomposition of copper (I) complexes with heterocyclic thiones. Journal of thermal analysis and calorimetry, 2011, 104.3: 1045-1050.
- [32] . Waseda, Yoshio, Eiichiro Matsubara, and Kozo Shinoda. X-ray diffraction crystallography: introduction, examples and solved problems. Springer Science & Business Media, 2011.
- [33] . Ballhausen, C. J. (1962). Introduction to Ligand Field Theory; McGraw-Hill: New York.
- [34] . Lever, A. B. P. (1984). Inorganic Electronic Spectroscopy.
- [35] . Synthesis and Characterization of Copper(II), Cobalt(II), Nickel(II), and Zinc(II) Complexes with Diketone Ligands.
- [36] . Hathaway, B. J. (1973). Structure and Bonding, 14, 60-120.
- [37] Figgis, B. N.; Hitchman, M. A. (2000). Ligand Field Theory and Its Applications.
- [38] Ballhausen, C. J. (1962). Introduction to Ligand Field Theory.
- [39] . Guo, H.; Xie, Y.; Chen, W. (2007). J. Mol. Struct., 841, 51-56.
- [40] SAEED, M.; SALEEM, R.; KHALID, Z. Synthesis and Chemical Characterization of Metals (Al, Cr, Co, Mn and VO) Complexes with Acetylacetone (β-diketone). J. Nat. Sci. Reserach, 2017, 7: 49-55.
- [41] . Cotton, F. A.; Wilkinson, G. (1999). Advanced Inorganic Chemistry.
- [42] . Reedijk, J., & Bouwman, E. (1999). Bioinorganic Catalysis. CRC Press.
- [43] Kaim, W., & Schwederski, B. (2010). Bioinorganic Chemistry: Inorganic Elements in the Chemistry of Life. Wiley.
- [44] . H. Syaima, S. B. Rahardjo and I. M. Zein, IOP Conf. Ser. Mater. Sci. Eng., 2018, 349, 1, pp. 012025-012031.
- [45] . AFFAT, Sajda; AL-SHAMKHAWY, Saher; SNIGUR, Denys. Cloud Point Extraction Coupled to Flame Atomic Absorbance Spectroscopy for Cobalt (II) determination with Azo-Azomethine Dye. University of Thi-Qar Journal of Science, 2024, 11.1: 124-130.
- [46] . AL-SAADAWY, Nuha H. Preparation and Characterization of novel metal complexes containing hydrazone derived from camphor and 2, 4-dinitrophenyl hydrazine. University of Thi-Qar Journal of Science, 2016, 6.1: 45-54.
- [47] M. R. Wasielewski, Chemical Reviews, 92 (1992) 435-461.
- [48] . H. D. Abruna et al., Journal of the American Chemical Society, 103 (1981) 1-5.
- [49] . B. S. Brunschwig et al., Journal of the American Chemical Society, 102 (1980) 579-586.
- [50] . J. P. Sauvage et al., Journal of the American Chemical Society, 113 (1991) 6110-6112.